Integrated Liver and Plasma Proteomics in Obese Mice Reveals Complex Metabolic Regulation

Authors

Ben Stocks, Alba Gonzalez-Franquesa, Melissa L. Borg, Marie Björnholm, Lili Niu, Juleen R. Zierath, and Atul S. Deshmukh

Correspondence

atul.deshmukh@sund.ku.dk

Graphical Abstract

In Brief

Obesity leads to the development of type 2 diabetes and nonalcoholic fatty liver disease. To identify the underlying processes of obesity-induced metabolic dysfunction, we performed proteomics in liver and plasma of *ob/ob* mice. Peroxisomal biogenesis and dysregulation of the secretory machinery were apparent in the liver of obese mice, alongside substantial alterations to the plasma proteome. Integration of these datasets identified putatively liver-derived proteins that are systemically dysregulated in obesity, many of which are also altered in human metabolic diseases.
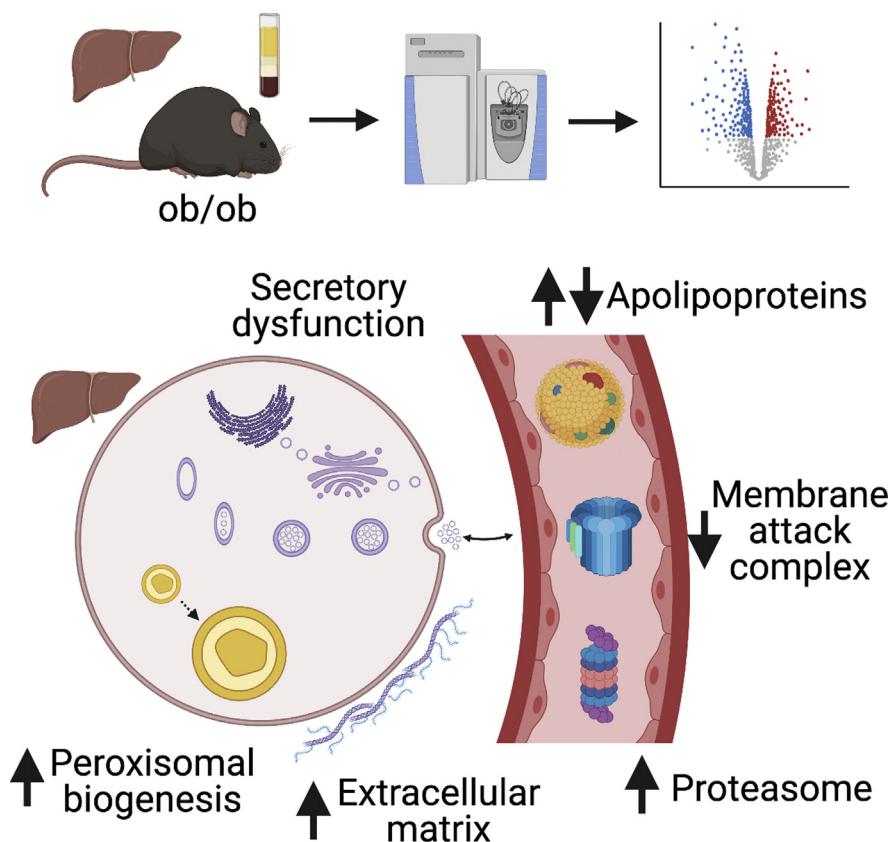
Highlights

- Proteomics reveals liver-derived proteins systemically dysregulated in obesity.
- Obesity increases hepatic lipid metabolism *via* peroxisomal biogenesis.
- Obesity dysregulates secretory machinery and secreted proteins within the liver.
- Metabolic and immune proteins dysregulated in plasma of obese mice.
- Comparative proteomics of high-fat diet and monogenic (*ob/ob*) models of obesity.

Integrated Liver and Plasma Proteomics in Obese Mice Reveals Complex Metabolic Regulation

Ben Stocks[1], Alba Gonzalez-Franquesa[1], Melissa L. Borg[2], Marie Björnholm[3], Lili Niu[4], Juleen R. Zierath[1,2,3], and Atul S. Deshmukh[1,4,*]

Obesity leads to the development of nonalcoholic fatty liver disease (NAFLD) and associated alterations to the plasma proteome. To elucidate the underlying changes associated with obesity, we performed liquid chromatography–tandem mass spectrometry in the liver and plasma of obese leptin-deficient *ob/ob* mice and integrated these data with publicly available transcriptomic and proteomic datasets of obesity and metabolic diseases in preclinical and clinical cohorts. We quantified 7173 and 555 proteins in the liver and plasma proteomes, respectively. The abundance of proteins related to fatty acid metabolism were increased, alongside peroxisomal proliferation in *ob/ob* liver. Putatively secreted proteins and the secretory machinery were also dysregulated in the liver, which was mirrored by a substantial alteration of the plasma proteome. Greater than 50% of the plasma proteins were differentially regulated, including NAFLD biomarkers, lipoproteins, the 20S proteasome, and the complement and coagulation cascades of the immune system. Integration of the liver and plasma proteomes identified proteins that were concomitantly regulated in the liver and plasma in obesity, suggesting that the systemic abundance of these plasma proteins is regulated by secretion from the liver. Many of these proteins are systemically regulated during type 2 diabetes and/or NAFLD in humans, indicating the clinical importance of liver–plasma cross talk and the relevance of our investigations in *ob/ob* mice. Together, these analyses yield a comprehensive insight into obesity and provide an extensive resource for obesity research in a prevailing model organism.

Obesity can lead to a multitude of chronic liver conditions, collectively known as nonalcoholic fatty liver disease (NAFLD). NAFLD encompasses increased hepatic triglyceride storage (steatosis) with or without liver inflammation (steatohepatitis) (1) and the possible progression to cirrhosis and/or hepatocellular carcinoma (2). Furthermore, dysregulated hepatic triglyceride metabolism contributes to insulin resistance and the development of type 2 diabetes alongside obesity (3, 4). In turn, insulin resistance may also contribute to the pathogenesis and development of fatty liver by leading to increased adipose tissue lipolysis and *de novo* lipogenesis in the liver (5). Obesity is considered an epidemic (6) with 13% of the world's adult population classified as obese (Global Health Observatory, 2017). At the same time, NAFLD has a 25% prevalence in Western and Asian populations (7, 8), raising to 80% to 90% in obese individuals (7). Hence, obesity and NAFLD are substantial global health challenges and understanding the molecular drivers and implications of obesity-related liver dysfunction is of increasing importance.

Obesity is characterized by chronic systemic inflammation and impaired immune function (9, 10). Although white adipose tissue is purported to be a major source of obesity-induced inflammation (11), the liver secretes the majority of highly abundant systemic proteins, including those involved in immune function (10). Thus, the development of liver dysfunction alongside obesity exerts considerable influence upon the plasma proteome (12) and, likely, the immune system. Obesity is also associated with the development of cardiovascular disease, Alzheimer's disease, and cancer (13–15). Indeed, liver dysfunction is emerging as a contributing factor to several diseases whereby the primary pathogenesis occurs in nonhepatic tissues (16–19).

The *ob/ob* mouse is a widespread model organism for obesity research (20), which harbors a mutation in the leptin gene (21–23). Leptin is a circulating adipose tissue-derived hormone that, among other things, signals to the hypothalamus, ultimately conveying information regarding energy storage and results in the modulation of feeding behaviors (24). Within 4 weeks of age, *ob/ob* mice develop obesity, insulin resistance, and hepatic steatosis (25, 26). Thus, *ob/ob* mice

are a conventional model organism for studying obesity, type 2 diabetes, and liver dysfunction.

Mass spectrometry–based proteomics provides a powerful tool to study (mal)adaptations across multiple tissues and biological fluids in pathophysiological conditions, such as obesity. Nonetheless, proteomics remains challenging in many tissues and fluids, such as liver and plasma, owing to their large dynamic range of protein abundance, in which highly abundant proteins hinder the detection of proteins with a low abundance. Here, we quantified the abundances of 7173 and 555 proteins within the liver and plasma of *ob/ob* mice and C57BL/6J lean control mice, providing biological insight into obesity and the hepatic alterations associated with NAFLD development, as well as a resource for the obesity research community. The *ob/ob* mice displayed liver and plasma proteomes that indicate impaired metabolism and immune function. Furthermore, we integrated the liver and plasma proteomes and identified circulating proteins putatively influenced by altered hepatic secretion during obesity and mapped their regulation in human metabolic diseases (*e.g.*, type 2 diabetes and NAFLD) and interventions (*e.g.*, diet and gastric bypass).

EXPERIMENTAL PROCEDURES
Animal Experiments

All animal experiments were approved by the Regional Animal Ethical Committee (Stockholm, Sweden). Four-month-old male *ob/ob* mice (21) and wild-type (WT) lean controls on a C57BL/6J background (liver samples: Charles River, Italy; plasma samples: Janvier Labs, France) had free access to water and standard rodent chow and were maintained in a temperature- and light-controlled (22–24 °C, 12-h light/dark cycle) environment. For the analysis of the liver proteome, mice were fasted for 4 h prior to anesthetization with Avertin (2,2,2-tribromoethanol 99% and tertiary amyl alcohol [1:1 w/v], 500 mg·kg^{-1} body weight). Livers were removed, frozen in liquid nitrogen, and stored at –80 °C until processing. For study of the plasma proteome, blood samples were collected into EDTA-coated tubes *via* tail blood sampling in the fed state. Blood samples were subjected to centrifugation at 12,000*g* for 5 min at 4 °C, and the plasma supernatant was collected and stored at –80 °C until processing.

Mass Spectrometry Sample Preparation and Measurement

Liver—Liver samples from *ob/ob* mice were prepared for mass spectrometry as described for skeletal muscle (27). Briefly, approximately 50 mg of liver (n = 4 per group) was homogenized in 750 µl of SDS buffer (0.1 M Tris-HCl, pH 7.5, 0.1 M DTT and 4% SDS) with an Ultra-Turrax homogenizer (IKA) and boiled at 95 °C for 5 min. Lysates were sonicated using a Branson tip-sonicator and subjected to centrifugation at 16,000*g* for 10 min. The supernatant was collected and 200 µg proteins was processed according to the multienzyme digestion with filter-aided sample preparation (MED-FASP) protocol using LysC (1:100 enzyme to protein ratio) and trypsin (1:100 enzyme to protein ratio) (28). Peptides (10 µg) originating from trypsin and LysC digests were purified on 2 × C18 StageTips (29). Peptides were separated on a 50-cm C18 column (inner diameter 75 µm, 1.8 µm beads, Dr. Maisch GmbH) and measured *via* liquid chromatography–tandem mass spectrometry (LC-MS/MS) using an Easy nano-flow

HPLC coupled *via* a nanoelectrospray ion source to a Q Exactive mass spectrometer (Thermo Fisher Scientific) using data-dependent acquisition. Peptides obtained from the LysC and Trypsin fractions were loaded onto the column with buffer A (0.5% formic acid) and eluted with a 270-min linear gradient increasing from 2% to 60% buffer B (80% acetonitrile, 0.5% formic acid). After the gradient, the column was washed with 95% buffer B and re-equilibrated with buffer A. The mass spectra were acquired in positive ion mode with automatic switching between mass spectrometry (MS) and MS/MS using a top 5 method. MS spectra were acquired in the Orbitrap analyzer with a mass range of 300 to 1750 *m/z* at a resolution of 70,000 with a target of 3 × 10^6 ions and a maximum injection time of 20 ms. Higher-energy C-trap dissociation peptide fragments acquired at 25 normalized collision energy were analyzed at a resolution of 17,500 in the Orbitrap analyzer with a target of 1 × 10^5 ions and a maximum injection time of 120 ms. Peptides were measured in singleton.

Plasma—Plasma samples from *ob/ob* mice were prepared for mass spectrometry as described (30) with minor modifications. Briefly, 1 µl of plasma was mixed with 24 µl of PreOmics lysis buffer (P.O. 00001, PreOmics GmbH) and boiled at 95 °C for 10 min. Proteins were digested with LysC (1:100 enzyme to protein ratio) for 1 h at 37 °C prior to the addition of trypsin (1:100 enzyme to protein ratio) for overnight digestion at 37 °C. About 10 to 15 µg of peptides were purified on 3 × styrenedivinylbenzene–reverse phase sulfonate StageTips. Peptides were separated on a 15-cm C18 column (inner diameter 75 µm, 1.8 µm beads, Dr. Maisch GmbH) and measured *via* LC-MS/MS using an Easy nano-flow HPLC coupled *via* a nano-electrospray ion source to a Q Exactive HF-X mass spectrometer (Thermo Fisher Scientific) using data-independent acquisition (DIA). Peptides were loaded onto the column with buffer A (0.5% formic acid) and eluted with a 45-min linear gradient increasing from 3% to 35% buffer B (80% acetonitrile, 0.5% formic acid). After the gradient, the column was washed with 98% buffer B. The DIA method used for the plasma proteome measurements contained one full scan (350–1650 *m/z*, resolution = 120,000) at a target of 3 × 10^6 ions, followed by 22 windows with a resolution of 30,000 where precursor ions were fragmented with higher-energy collisional dissociation (stepped collision energy 25%, 27.5%, 30%) and analyzed with an automatic gain control target of 3 × 10^6 ions and maximum injection time at 54 ms in profile mode using positive polarity. Different proteomic methods were employed to measure the liver and plasma proteomes, reflecting the different characteristics of these biological matrixes (*e.g.*, tissue versus biofluid, sample complexity, and expected proteome depth) and the technological and methodological advances in proteomic analyses that occurred over the course of this investigation.

Mass Spectrometry Data Analyses

Liver Proteome—Raw MS files were analyzed using MaxQuant version 1.6.7.0 (31) (http://www.maxquant.org). MS/MS spectra were searched by the Andromeda search engine against the mouse FASTA database (version 2017_11, containing 69,720 entries from the SwissProt and TrEMBL databases) supplemented with 262 frequently observed contaminants and forward and reverse sequences. In the main Andromeda search precursor, mass and fragment mass were matched with an initial mass tolerance of 6 and 20 ppm, respectively. Minimum score for modified and unmodified peptides were set at 0 and 40, respectively. The search included variable modifications of methionine oxidation and N-terminal acetylation and fixed modification of carbamidomethyl cysteine. The specific digestion method was set as "LysC" for the first Lys-C-derived fraction and "Trypsin/P" for the second trypsin-derived fraction. Minimal peptide length was set to seven amino acids, and a maximum of two miscleavages were allowed. The false discovery rate (FDR) was set to 0.01 for peptide and protein identifications. MS runs were analyzed with the "match

between runs" option, with a retention time window of 30 s. When all identified peptides were shared between two proteins, results were combined and reported as one protein group. Matches to the reverse database were excluded.

Plasma Proteome—Plasma proteome files acquired in DIA mode were processed using Biognosys Spectronaut software version 12 (32). DIA raw data were analyzed using an in-house generated spectral library of mouse plasma that contains 11,566 peptides and 1461 protein groups (supplemental Table S1; mouse UniProt FASTA database, version 2018_06, containing 92,096 entries) (33). The experimental DIA runs were analyzed in Spectronaut using default settings. The mass tolerance for the precursor ion envelope in MS1 was determined from the data using a calibration search, with a starting width of 20 ppm. For peptide identification, the six most intense fragment ions are selected (minimally three when less than six fragment ions are apparent). The mass tolerance for the main library search is determined from the data using a calibration search, with a starting width of 20 ppm (for MS1 and MS2 separately). FDR was calculated run-wise at the precursor level and experiment-wide on the protein group level using the Storey method (34).

Bioinformatics Analyses

Bioinformatics analyses were performed on MaxQuant raw intensities for liver proteomes and on Spectronaut intensities for plasma proteomes. Bioinformatics analysis was performed in the Perseus software (35) unless otherwise stated. For the liver proteome, relative protein quantification was performed *via* the total protein abundance (TPA) methodology, whereby the raw protein intensity values were divided by the total protein intensity in a sample (36, 37); all analyses in the liver proteome were performed on $\log_2$-transformed TPA values. TPA values were multiplied by 10^8 prior to $\log_2$-transformation to ensure positive $\log_2$ values were displayed in figures. Categorical annotation was supplied in the form of gene ontology (GO) biological process (GOBP), gene ontology cellular component (GOCC), Kyoto encyclopedia of genes and genomes (KEGG) pathway and UniProt keyword terms. All annotations were extracted from the UniProt database. Protein data were filtered to remove proteins identified with only a single modified peptide "only identified by site," reverse sequences, and potential contaminants and to have >60% coverage in at least one group (Liver proteome: three of four, plasma proteome: four of seven). Data were imputed to fill missing abundance values by drawing random numbers from a Gaussian distribution with a standard deviation of 30% and a downshift of 1.8 standard deviations from the mean relative to that of the proteome abundance distribution. Two sample *t* tests were performed on WT and *ob/ob* groups with a permutation-based FDR and an S0 of 0.1 applied (38). Summed protein abundances were calculated by summing the total protein abundance values for each protein annotated to a particular GO term. Overrepresentation enrichment analyses were performed using the ClueGo App on Cytoscape (39) using a right-sided hypergeometric test (Benjamini–Hochberg FDR <0.02) (40) in significantly regulated proteins compared with the whole proteome. Additional enrichment analyses were performed using a one-dimensional enrichment analysis (40), in which protein $\log_2$-fold change values were ranked and a test was performed for each annotation term to determine whether the $\log_2$-fold change for the proteins belonging to the annotation were systemically larger (positive enrichment) or smaller (negative enrichment) than the global distribution of all the $\log_2$-fold change for all the proteins. Proteomic data from the liver of *ob/ob* mice were compared with publicly available datasets, including the *ob/ob* liver transcriptome (41) and the liver proteome of high-fat diet (HFD)-fed mice (42). Enrichment of GO terms and KEGG pathways were compared in each dataset using a two-dimensional enrichment analysis (40).

Hierarchical clustering analysis was performed using Euclidean distance (41, 42).

Physiological Phenotyping

Mice were single housed in individual Plexiglas cages of the Comprehensive Lab Animal Monitoring System (CLAMS; Columbus Instruments), and food intake, locomotor activity, and oxygen consumption were continuously monitored. During the CLAMS session, mice were maintained on a 12:12-h light–dark cycle and had free access to standard rodent chow and water. Glucose tolerance was assessed using an intraperitoneal glucose tolerance test after a 4-h fast, as described (43).

Experimental Design and Statistical Rationale

Liver samples were analyzed from four mice per genotype (biological replicates). Plasma samples were analyzed from seven mice per genotype (biological replicates). Statistical power was deemed to be sufficient based on our previous observations in skeletal muscle of *ob/ob* mice (27). Student's *t* tests were used to compare means after log-transformation and visual inspection of normal distribution. For physiological data, independent Student's *t* test or two-way analysis of variance, with Ryan–Holm–Bonferroni corrections where appropriate, were used to assess differences between genotypes and interactions with time.

RESULTS

High Coverage and Reproducibility of Liver and Plasma Proteomes

We performed LC-MS/MS on liver and plasma samples from leptin-deficient *ob/ob* mice and wild-type C57BL/6J controls (Fig. 1*A*). *ob/ob* mice were obese and glucose intolerant, displaying elevated body mass, food intake, blood glucose, and plasma insulin, as well as reduced activity and maximal oxygen uptake (supplemental Fig. S1, *A–F*). We identified 7684 proteins from two fractions using the MED-FASP protocol (28) (supplemental Table S2). Filtering for three valid values (out of four) in at least one genotype resulted in the final quantification of 7173 proteins (supplemental Table S3). The number of quantified proteins per sample ranged between 6427 and 6911 (supplemental Fig. S2*A*). Good reproducibility between biological replicates was apparent (Pearson's r range: 0.89–0.98), which was higher than between samples from different genotypes (Pearson's r range: 0.86–0.93) (supplemental Fig. S2*B*). Proteins were quantified across a wide range of TPA values, with six orders of magnitude between the highest and lowest abundant quantified proteins (supplemental Fig. S2*C*). The quantified proteins included several transcription factors (*e.g.,* ARNTL (BMAL1), CLOCK, CREB1, FOXO1, HNF1A, HNF4A, and PPARA), which are challenging to quantify in tissue owing to their low protein abundance.

Plasma samples were prepared for proteomics in a single fraction (Fig. 1*A*), as described (30). We identified 592 proteins in plasma (supplemental Table S4). Intensities were filtered for four valid values (out of seven) in at least one genotype, resulting in the final quantification of 555 proteins (supplemental Table S5). The number of quantified proteins
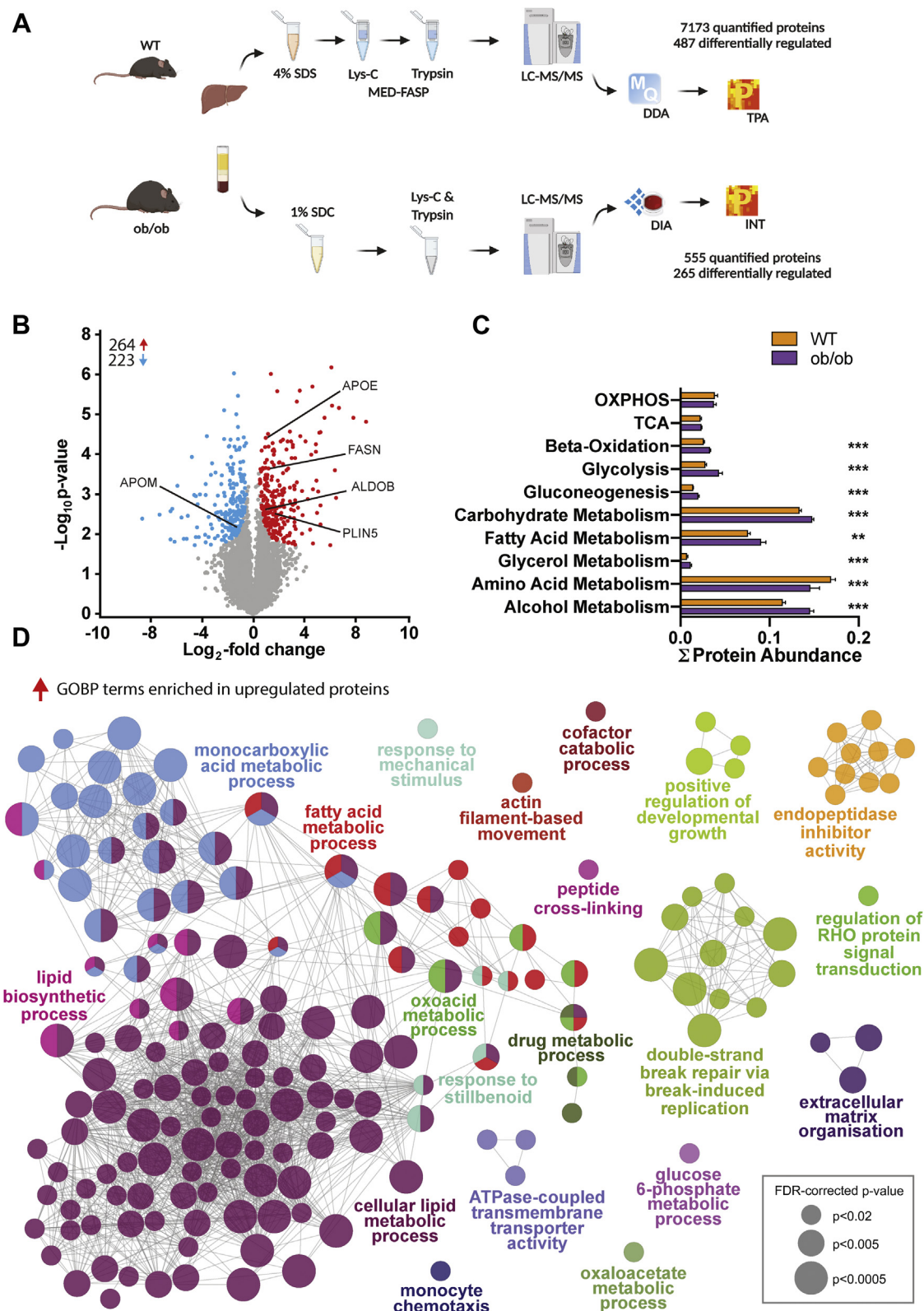
FIG. 1. **Lipid metabolic processes are increased in the liver of *ob/ob* mice.** *A, ob/ob* mice and wild-type (WT) controls were sacrificed for liver (n = 4) and plasma (n = 7) proteomics. Liver samples were prepared using the multienzyme digestion with filter-aided sample preparation (MED-FASP) protocol (28) and measured with a data-dependent acquisition (DDA) method. The resulting spectra were analyzed by MaxQuant software and were quantified using the total protein abundance (TPA) approach (36). Plasma samples were measured with a data-independent

per sample ranged between 426 and 516 (supplemental Fig. S2D). Good reproducibility between biological replicates was also apparent in the plasma proteome (Pearson's r range: 0.87–0.95), which was substantially higher than between samples from different genotypes (Pearson's r range: 0.78–0.85) (supplemental Fig. S2E). Similarly to the liver proteome, proteins were quantified across approximately five orders of magnitude (supplemental Fig. S2F), demonstrating the large dynamic range of the liver and plasma proteomes.

The Liver Proteome of ob/ob Mice Displays Elevated Lipid Metabolic Processes

Of the 7173 quantified liver proteins, 487 proteins were differentially regulated (FDR <0.05, S0 = 0.1), with 264 proteins upregulated and 223 proteins downregulated within the liver of ob/ob mice (Fig. 1B and supplemental Table S3). These included fructose-biphosphate aldolase B (ALDOB), an enzyme involved in glycolysis and gluconeogenesis, as well the apolipoproteins E (APOE) and M (APOM). Furthermore, fatty acid synthase (FASN) and the lipid droplet protein perilipin-5 (PLIN5) were among the upregulated proteins. To assess the effect of obesity on aspects of metabolism, the abundance of proteins annotated to various GOBP terms were summed and compared between groups (Fig. 1C). Increased summed protein abundance of processes involved in fat metabolism (e.g., β-oxidation, fatty acid metabolic process, glycerol metabolic process), carbohydrate metabolism (e.g., glycolysis, gluconeogenesis, and carbohydrate metabolic process), and alcohol metabolism were observed in liver from ob/ob mice (Fig. 1C). Conversely, the summed protein abundance for proteins annotated to amino acid metabolic process was decreased (Fig. 1C). Despite the increase in summed protein abundance related to substrate metabolism, neither oxidative phosphorylation (OXPHOS) nor the tricarboxylic acid cycle was affected (Fig. 1C).
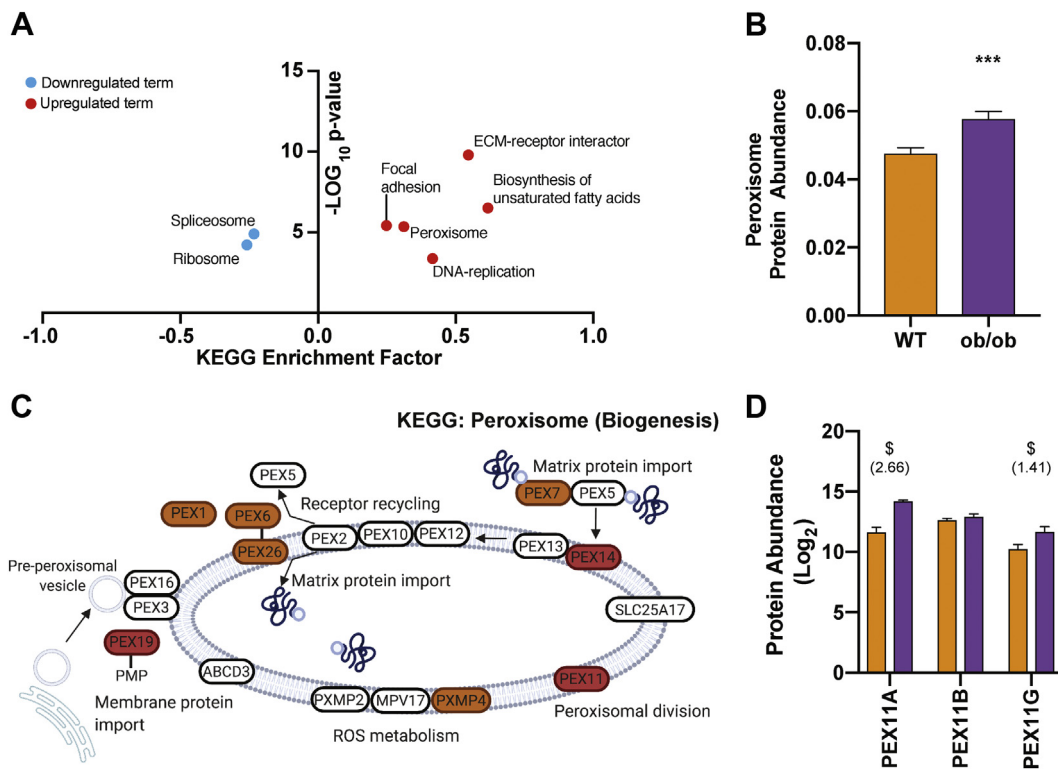
To systematically identify proteomic changes to biological processes, we performed enrichment analyses for GOBP terms in the upregulated and downregulated proteins using ClueGO (39). No GOBP terms were significantly enriched in the downregulated proteins; however, a multitude of GOBP terms were enriched within the upregulated proteins (Fig. 1D and supplemental Table S6). Groups of enriched terms and their interactions are displayed in Figure 1D. The largest cluster of enriched terms are primarily related to fatty acid metabolism, including fatty acid metabolic process, cellular lipid metabolic process, lipid biosynthetic process, and monocarboxylic acid metabolic process. Additional biological processes enriched within the upregulated proteins included terms related to glucose-6-phosphate metabolism, double-strand break repair via break-induced replication, and extracellular matrix organization (Fig. 1D and supplemental Table S6). Thus, changes to the ob/ob liver proteome are primarily related to the metabolism of fatty acids.

Peroxisomal Biogenesis in the Liver of ob/ob Mice

In line with the enriched GOBP terms related to fatty acid metabolism, the KEGG terms biosynthesis of unsaturated fatty acids and peroxisome were enriched within the upregulated proteins (Fig. 2A and supplemental Table S7). In addition, summed protein abundance of the GOCC term peroxisome was increased (Fig. 2B). This is complementary to elevated fatty acid metabolic processes in the absence of changes to mitochondrial processes in both the summed protein abundance (Fig 1C and supplemental Fig. S3) and GOBP enrichment (Fig. 1D) analyses. Together, these results implicate the peroxisome as the site of elevated fatty acid metabolism within ob/ob liver; thus, we investigated the mediators of peroxisomal biogenesis in further detail (Fig. 2C and supplemental Fig. S4A). Peroxisomal biogenesis encompasses the import of peroxisomal membrane and matrix proteins and the elongation and division of existing peroxisomes (44). Peroxisomal biogenesis factor (PEX) 19, which binds newly synthesized peroxisomal membrane proteins and shuttles them to the membrane protein import machinery (45), was increased in liver from ob/ob mice. PEX3 and PEX16, which are also required for de novo peroxisomal biogenesis (44) remained unchanged (Fig. 2C). Of the proteins involved in the import of peroxisomal matrix proteins, PEX7 increased at a less stringent false discovery rate (FDR < 0.10), whereas PEX5, the other cytosolic peroxisomal matrix protein receptor (44), remained unchanged. PEX14, which PEX5 and PEX7 dock to during peroxisomal matrix protein import, increased in the absence of changes to its docking complex partner PEX13. PEX1, PEX6, and PEX26, which mediate the recycling of peroxisomal matrix protein receptors (44), were all increased at an FDR < 0.10 (Fig. 2C). Peroxisomal elongation and division is initiated via PEX11 isoforms, which recruit the fission proteins dynamin-1-like protein (DNM1L), mitochondrial fission 1 protein (FIS1), and mitochondrial fission factor (MFF) (46). PEX11A and PEX11G were increased in ob/ob liver, although PEX11B was unaltered (Fig. 2D, isoforms quantified with unique peptides). Changes to PEX11 isoforms

Fig. 2. **Peroxisomal proliferation in the liver of *ob/ob* mice.** *A*, one-dimensional enrichment analysis based on Kyoto encyclopedia of genes and genomes (KEGG) pathways (FDR < 0.02). *B*, summed protein abundance of the gene ontology cellular compartment (GOCC) term *peroxisome*. *C*, partial reproduction of the KEGG *Peroxisome* pathway, showing proteins involved in peroxisomal biogenesis with proteins denoted as upregulated or downregulated at an FDR < 0.05 or 0.10. *D*, protein abundance of PEX11 isoforms. Data are represented as mean ± SD (n = 4), permutation-based FDR-corrected Student's *t* test (proteome): $^{\$}$FDR < 0.05, Student's *t* test (summed protein abundance): ***p < 0.001.

occurred in the absence of significant changes to the peroxisomal fission proteins DNM1L, FIS1, and MFF, although MFF displayed a nonsignificant decrease in protein abundance (q = 0.103; supplemental Fig. S4*B*).

Obesity Dysregulates Secretory Machinery and Secreted Proteins Within the Liver

A one-dimensional enrichment analysis of GOCC terms identified systematic regulation of cellular compartments involved in protein secretion (supplemental Table S8). *Endoplasmic reticulum chaperone complex* was enriched within the downregulated proteins (Fig. 3*A*), whereas *extracellular vesicle exosome* and *extracellular matrix* were enriched within the upregulated proteins (Fig. 3*A*). Protein secretion is mediated *via* different secretory pathways (*i.e.*, classical secretion or nonclassical secretion). Thus, we investigated these secretory pathways in further detail. Classically secreted proteins contain an endoplasmic reticulum–targeting signal peptide (47). The majority of signal peptide–containing proteins are transported *via* vesicles through the endoplasmic reticulum and the Golgi apparatus and are released into the extracellular space by vesicular fusion with the plasma membrane (48). Within the liver proteome, we quantified 741 proteins

annotated to contain a signal peptide (UniProt Keyword: *signal peptide*) (Fig. 3*B*). Of these, 79 were differentially regulated with 38 upregulated and 41 downregulated in the liver of *ob/ob* mice (Fig. 3*B*). The signal peptide–containing proteins with the highest positive and negative fold-changes are identified in Figure 3*B*; these include the upregulation of Interferon gamma receptor 1 (INGR1) and Interferon alpha-inducible protein 27-like protein 2B (IFI27L2B), indicating liver damage–associated interferon signaling (49, 50) in *ob/ob* mice. In line with the enrichment of the *endoplasmic reticulum chaperone complex* within the downregulated proteins, five of the ten quantified proteins within the *endoplasmic reticulum chaperone complex* were significantly downregulated (Fig. 3*C*), whereas the summed protein abundance of the endoplasmic reticulum was also decreased (supplemental Fig. S3). Furthermore, the total abundance of proteins annotated to the Golgi apparatus was increased in *ob/ob* mice (Fig. 3*D*). During nonclassical secretion, proteins are secreted *via* several mechanisms independently of the endoplasmic reticulum and the Golgi apparatus. One such mechanism is the secretion of exosomes, a form of extracellular vesicle (51). The GOCC term *extracellular vesicle exosome* was enriched within the upregulated proteins (Fig. 3*A*). Filtering for proteins
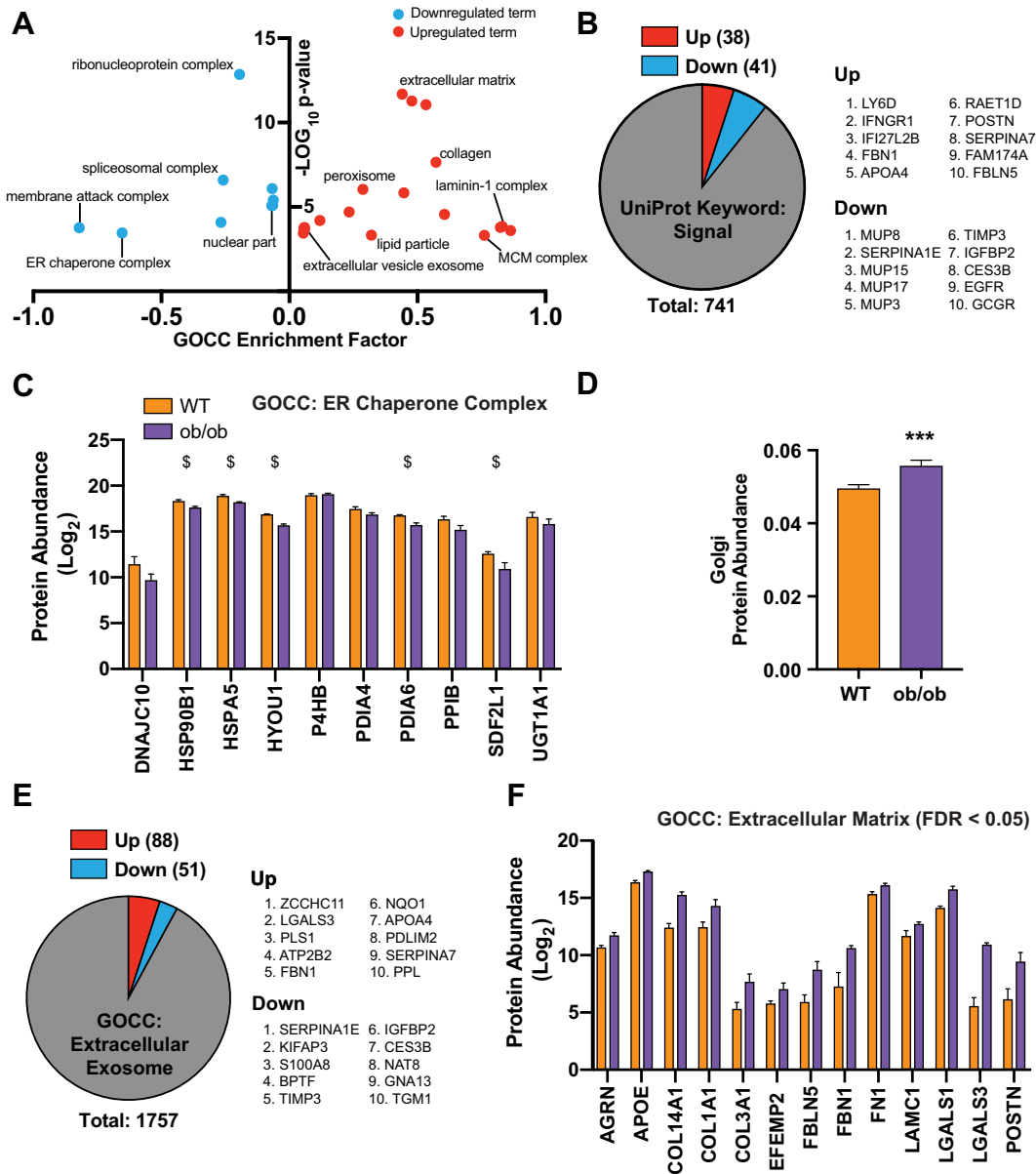
FIG. 3. **The secretory machinery and secreted proteins are dysregulated within the liver of *ob/ob* mice.** *A*, one-dimensional enrichment analysis based on GOCC terms (FDR < 0.02). *B*, regulation of proteins annotated to contain a *signal peptide* (UniProt Keyword). The ten proteins with the largest positive and negative fold-changes, respectively, are listed. *C*, protein abundance of the ten proteins annotated to the *endoplasmic reticulum chaperone complex* (GOCC) filtered from the proteome, of which five were significantly downregulated. *D*, summed protein abundance of the GOCC term *Golgi apparatus*. *E*, regulation of proteins annotated to *extracellular exosome* (GOCC). The ten proteins with the largest positive and negative fold-changes, respectively, are listed. *F*, protein abundance of the 13 significantly regulated proteins annotated to *extracellular matrix* filtered from the proteome. Data are represented as mean ± SD (n = 4), permutation-based FDR corrected Student's *t* test (proteome): $^{\$}$FDR < 0.05, Student's *t* test (summed protein abundance): ***p < 0.001. GOCC, gene ontology cellular compartment.

annotated to *extracellular vesicle exosome* (GOCC) resulted in the quantification of 1757 proteins within the liver that are putatively associated with exosomes (Fig. 3*E*). Of these, 88 and 51 proteins were significantly upregulated and downregulated, respectively. Among the most highly upregulated was galectin-3 (LGALS3) (Fig. 3*E*), a profibrotic extracellular matrix protein (52).

The *extracellular matrix* and related protein groups (*e.g.*, *collagen* and *laminin-1 complex*) were also enriched within the upregulated proteins (Fig. 3*A*). The significantly upregulated proteins within the GOCC term *extracellular matrix* are displayed in Figure 3*F*. The majority of these are structural proteins of the extracellular matrix (*e.g.*, collagen proteins COL1A1, COL3A1, and COL14A1; fibrillin 1 [FBN1]; fibronectin
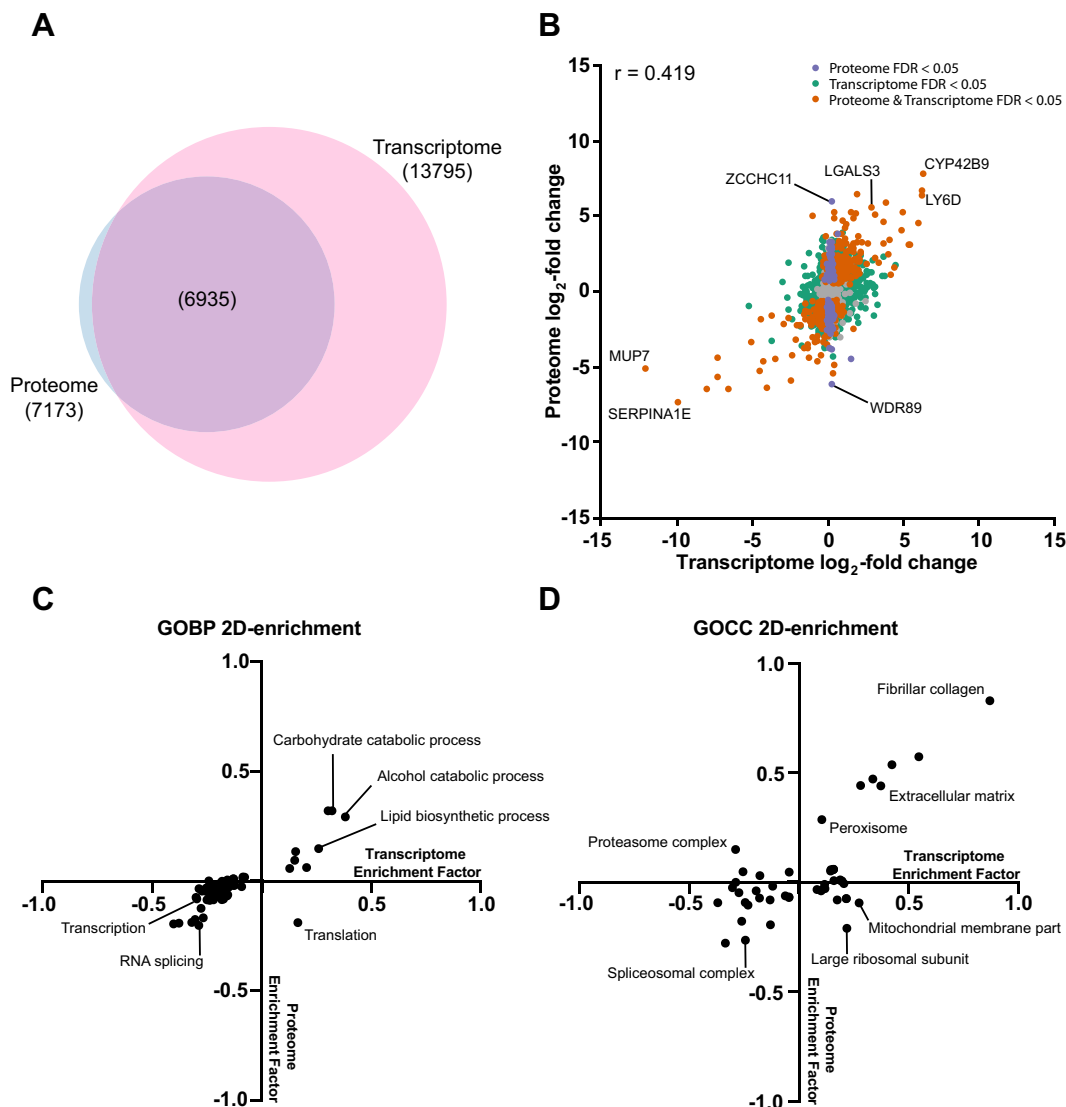
FIG. 4. **Transcriptional regulation of the liver proteome of *ob/ob* mice.** *A*, Venn diagram displaying the overlap of proteins and transcripts quantified in the liver proteome and a previously published transcriptome (41) of *ob/ob* mice. *B*, scatter plot of the log$_2$-fold change in the transcriptome and proteome. Proteins/transcripts significantly regulated only in the transcriptome or proteome are displayed in *green* and *purple*, respectively; proteins/transcripts significantly regulated in both the transcriptome and proteome are highlighted in *orange*. *C* and *D*, two-dimensional enrichment analysis based on GOBP (*C*) and GOCC (*D*) terms for the proteome and transcriptome (FDR < 0.02). GOBP, gene ontology biological processes; GOCC, gene ontology cellular compartment.

[FN1]; and laminin [LAMC1]), although a number of secreted proteins annotated to the extracellular matrix were also upregulated (*e.g.*, APOE, galectin-1 [LGALS1], LGALS3, and periostin precursor [POSTN]). All together, we demonstrate a substantial regulation of the secretory machinery and the extracellular matrix within the liver of *ob/ob* mice.

Transcriptional Regulation of the Liver Proteome of ob/ob *Mice*

To investigate the degree to which the observed changes in the liver proteome are transcriptionally regulated, we took advantage of our deep liver proteome and integrated it with a published transcriptomic dataset from the liver of *ob/ob* mice (41). Of the 7173 proteins we quantified in the liver, 6935 had corresponding transcripts quantified in the published transcriptome dataset (Fig. 4*A*). Correlation of the transcriptomic and proteomic log$_2$-fold changes compared with wild-type controls displayed only a moderate correlation (Fig. 4*B*; Pearson's r = 0.419). A total of 377 proteins/transcripts were differentially regulated in both transcriptome and the proteome. Indeed, the proteins with the largest changes in the proteome (both up- and downregulated) were also the most

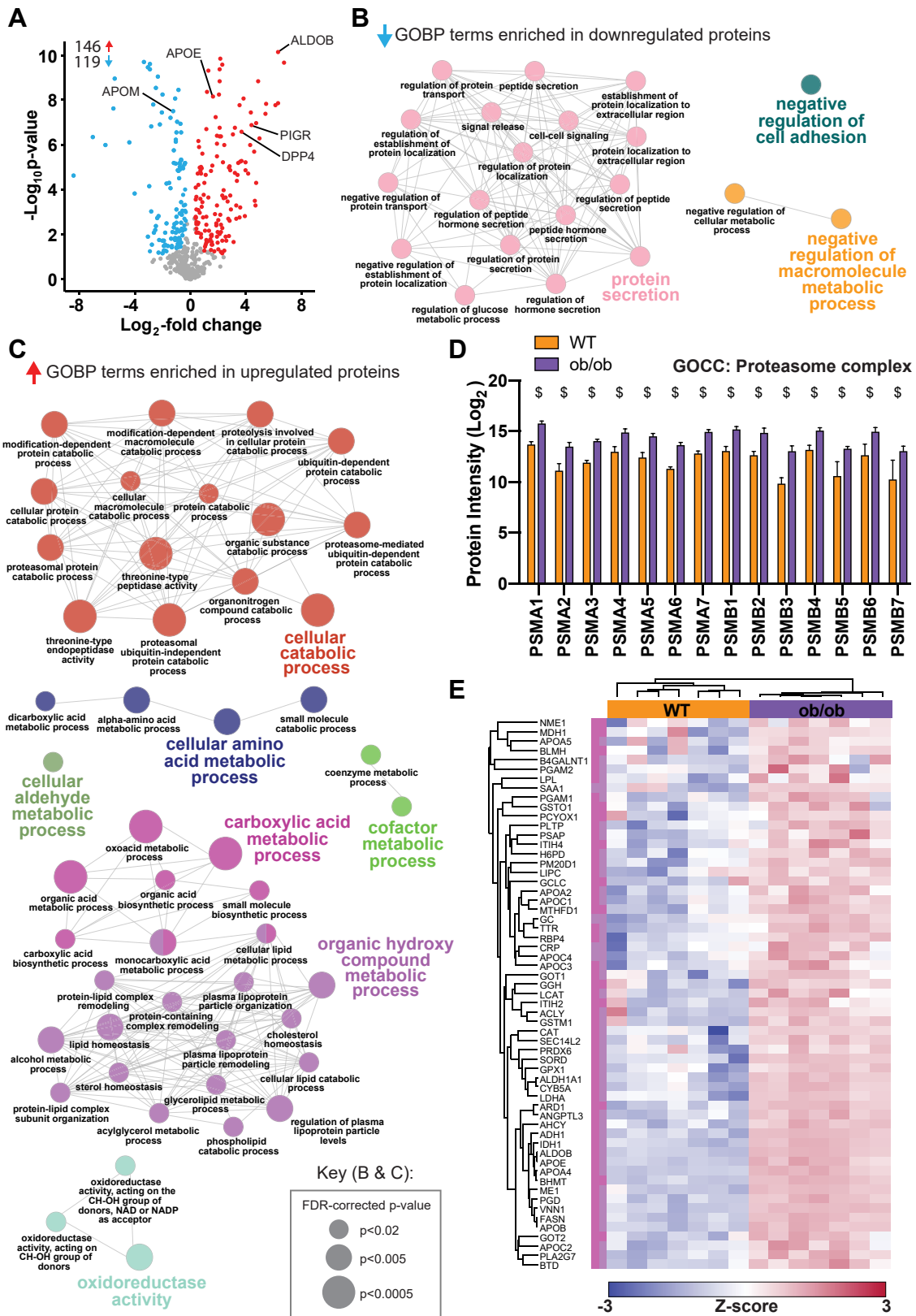FIG. 5. **Proteasomal proteins and lipid metabolic processes are increased in the plasma proteome of *ob/ob* mice.** *A*, volcano plot of the plasma proteome showing 146 significantly upregulated proteins in *red* and 119 significantly downregulated proteins in *blue* (FDR < 0.05, S0 = 0.1). *B* and *C*, functional enrichment analysis by ClueGO for the significantly downregulated (*B*) and upregulated (*C*) proteins. Right-sided

regulated at the transcriptional level (*e.g.*, SERPINA1E, MUP7, LY6D, and CYP42B9). However, there were 4018 differentially regulated transcripts that did not change at the protein level, whereas 97 proteins were regulated without changes in transcription. To identify concomitantly and divergently regulated cellular compartments and biological processes between the proteome and transcriptome, we performed a two-dimensional enrichment analysis and displayed how enriched terms were regulated in each dataset. The metabolic processes *carbohydrate catabolic process, lipid biosynthetic process*, and *alcohol catabolic processes* (GOBP) were positively enriched in both the transcriptome and the proteome, indicating substantial transcriptional control of these processes in obesity (Fig. 4C and supplemental Table S9). Similarly, GOCC terms relating to the *extracellular matrix* and *fibrillar collagen* displayed concordant regulation in the proteome and transcriptome, as was also the case with the *peroxisome* (Fig. 4D and supplemental Table S10). Conversely, terms related to the mitochondria, including *mitochondrial membrane part* (Fig. 4D), were upregulated at the transcriptional level but not in the proteome, whereas the ribosome is decreased in the proteome and moderately upregulated in the transcriptome (Figs. 2D and 4D). Thus, although some of the major metabolic pathways and cellular compartments that are regulated in the liver of *ob/ob* mice are driven by transcriptional regulation, posttranscriptional mechanisms (*e.g.*, translation and/or degradation) likely also regulate the liver proteome during obesity.

To validate our results and identify common obesity phenotypes between models, we compared the liver proteome of *ob/ob* mice (fed a chow diet) to a liver proteome derived from HFD-fed wild-type mice of the same age and genetic background (42). We observed only a very small correlation (Pearson's r = 0.158) between the log$_2$-fold changes observed in the liver of *ob/ob* and HFD-fed mice (supplemental Fig. S5A), indicating that changes at the individual protein level are markedly different between *ob/ob* mice and HFD-fed mice. However, when comparing systematic changes *via* two-dimensional enrichment analyses, we can identify cellular compartments, processes, and pathways that are similarly regulated in *ob/ob* and HFD-fed mice (supplemental Fig. S5B and supplemental Table S11). For example, terms related to fatty acid metabolism, glycolysis/gluconeogenesis, and peroxisomal proliferation were upregulated in both models of obesity. Conversely, terms related to the extracellular matrix (*e.g.*, *extracellular matrix* and *fibrillar collagen*) were divergently regulated, displaying substantial upregulation in the liver of *ob/ob* mice and downregulation in HFD-fed mice

(supplemental Fig. S4B). These concordant and divergent phenotypes are important to consider when choosing a model organism in obesity and/or NAFLD research.

ob/ob *Mice Exhibit a Dysregulated Plasma Proteome Enriched for Proteasomal and Metabolic Processes*

Of the 555 quantified plasma proteins, 265 proteins were significantly regulated (FDR <0.05, S0 = 0.1), with 146 proteins upregulated and 119 proteins downregulated in the plasma of *ob/ob* mice (Fig. 5A and supplemental Table S5). These included the upregulation of the clinical NAFLD markers ALDOB, APOE, dipeptidyl peptidase 4 (DPP4), and polymeric immunoglobulin receptor (PIGR) and the downregulation of APOM (12). We performed enrichment analyses based on GOBP terms enriched within the upregulated and downregulated proteins using ClueGO (39). GOBP terms enriched within the downregulated proteins were related to *protein secretion*, including *regulation of hormone secretion* and *regulation of glucose metabolic process*. These enriched terms were driven by the regulation of proteins such as adiponectin (ADIPOQ), annexin-a1 (ANXA1), epidermal growth factor receptor (EGFR), glycosylphosphatidylinositol-specific phospholipase D (GPLD1), and major urinary proteins (MUP1, MUP2, and MUP3). Terms related to *negative regulation of macromolecule metabolic process* and *negative regulation of cell adhesion* were also enriched in the downregulated proteins (Fig. 5B and supplemental Table S12). Enriched within the upregulated proteins were terms related to *cellular catabolic process* (Fig. 5C and supplemental Table S13), which was particularly driven by the coordinated upregulation of the 20S proteasome complex proteins in plasma (Fig. 5D). *Carboxylic acid metabolic process*, *lipid homeostasis*, *cholesterol homeostasis*, and *plasma lipoprotein organization* were all enriched within the enrichment term cluster depicted in the two shades of purple (Fig. 5C). Proteins driving the enrichment of these two clusters are shown in Figure 5E and are predominantly apolipoproteins, as well as proteins involved in glycolysis and the tricarboxylic acid cycle. Terms related to *cellular aldehyde metabolic process*, *cofactor metabolic process*, and *oxidoreductase activity* were also enriched in the upregulated proteins (Fig. 5C).

Impaired Coagulation and Complement Cascades in the Plasma of Obese Mice

KEGG enrichment analysis revealed that *complement and coagulation cascades* were enriched in the downregulated proteins (Fig. 6A and supplemental Table S14). Plasma proteomics allowed for the quantification of the majority of the

---

hypergeometric test, Benjamini–Hochberg FDR < 0.02, functionally related terms are grouped and color coded based on overlapping proteins. The most significantly regulated terms in each group are labeled in color. *D*, protein abundance of the ten proteins annotated to the *proteasome complex* (GOCC). *E*, hierarchical cluster of the proteins within the purple enrichment term groups (whose most significantly regulated terms were carboxylic acid metabolic process and organic hydroxyl compound metabolic process) in (*C*). Data are represented as mean ± SD (n = 7), permutation-based FDR-corrected Student's *t* test (proteome): $^\$$FDR < 0.05. GOCC, gene ontology cellular compartment.
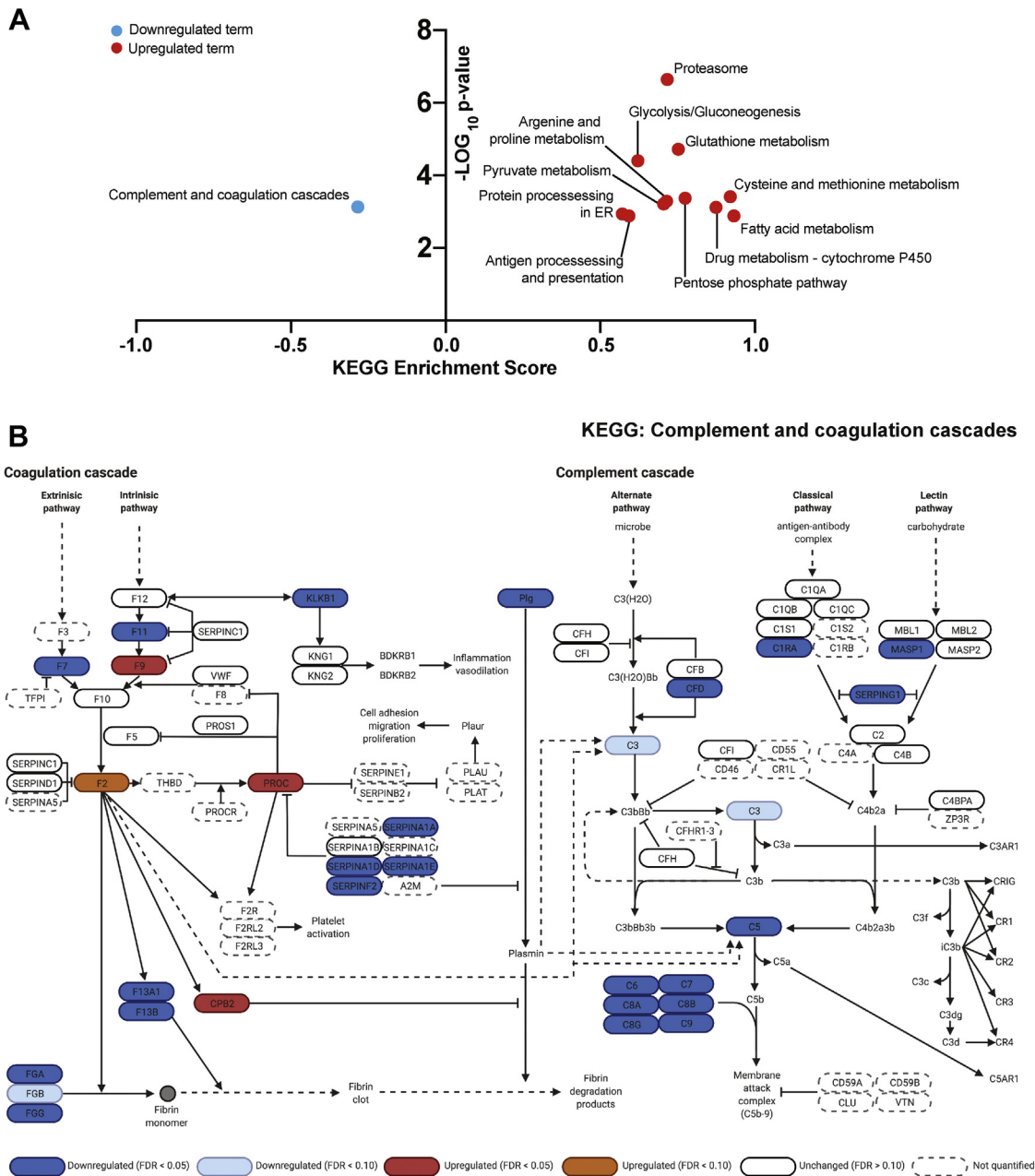

FIG. 6. **Downregulation of the complement and coagulation cascades in the plasma of *ob/ob* mice.** *A*, one-dimensional enrichment analysis based on KEGG terms (FDR < 0.02). *B*, reproduction of the KEGG *complement and coagulation cascades* pathway with proteins denoted as upregulated or downregulated at an FDR < 0.05 or 0.10. KEGG, Kyoto encyclopedia of genes and genomes.

proteins within the *complement and coagulation cascades* KEGG pathway (Fig. 6*B* and supplemental Fig. S6), which were predominantly downregulated in obesity. Hence, within the coagulation cascade, the fibrinogen subunits (FGA, FGB, and FGC) were downregulated alongside the coagulation factors F13A1 and F13B. Plasminogen, which degrades fibrin clots, was also decreased in the plasma of *ob/ob* mice. Furthermore, the protease inhibitors alpha-1-antitrypsin 1-1,

1-4, and 1-5 (SERPINA1A, SERPINA1D, and SERPINA1E, respectively) and alpha-1-antiplasmin SERPINF2 were also decreased. In the case of the complement cascade, plasma abundance of the terminal complement complex (complement components 5–9; C5–C9) was decreased. This was accompanied by a decrease in various protein precursors from the alternate pathway (*e.g.*, complement component 3; C3), the classical pathway (*e.g.*, complement subcomponent C1r;

C1RA), and the lectin pathway (*e.g.*, mannan-binding lectin serine protease 1; MASP1) (Fig. 6*B*).

Integrated Liver and Plasma Proteomics Reveal Putative Liver-Derived Proteins Dysregulated in the Plasma of ob/ob *Mice*

To identify proteins whose plasma abundance is likely to be regulated by altered secretion from the liver, we integrated the liver and plasma proteomes by looking for common features among the two datasets. Of the 7173 and 555 proteins quantified in liver and plasma, respectively, 224 proteins were quantified in both proteomes, of which 31 proteins were differentially regulated (FDR <0.05) in both liver and plasma (Fig. 7A). For proteins quantified in both liver and plasma, we plotted the log$_2$-fold change in each dataset on a scatter plot and highlighted the proteins that were significantly regulated
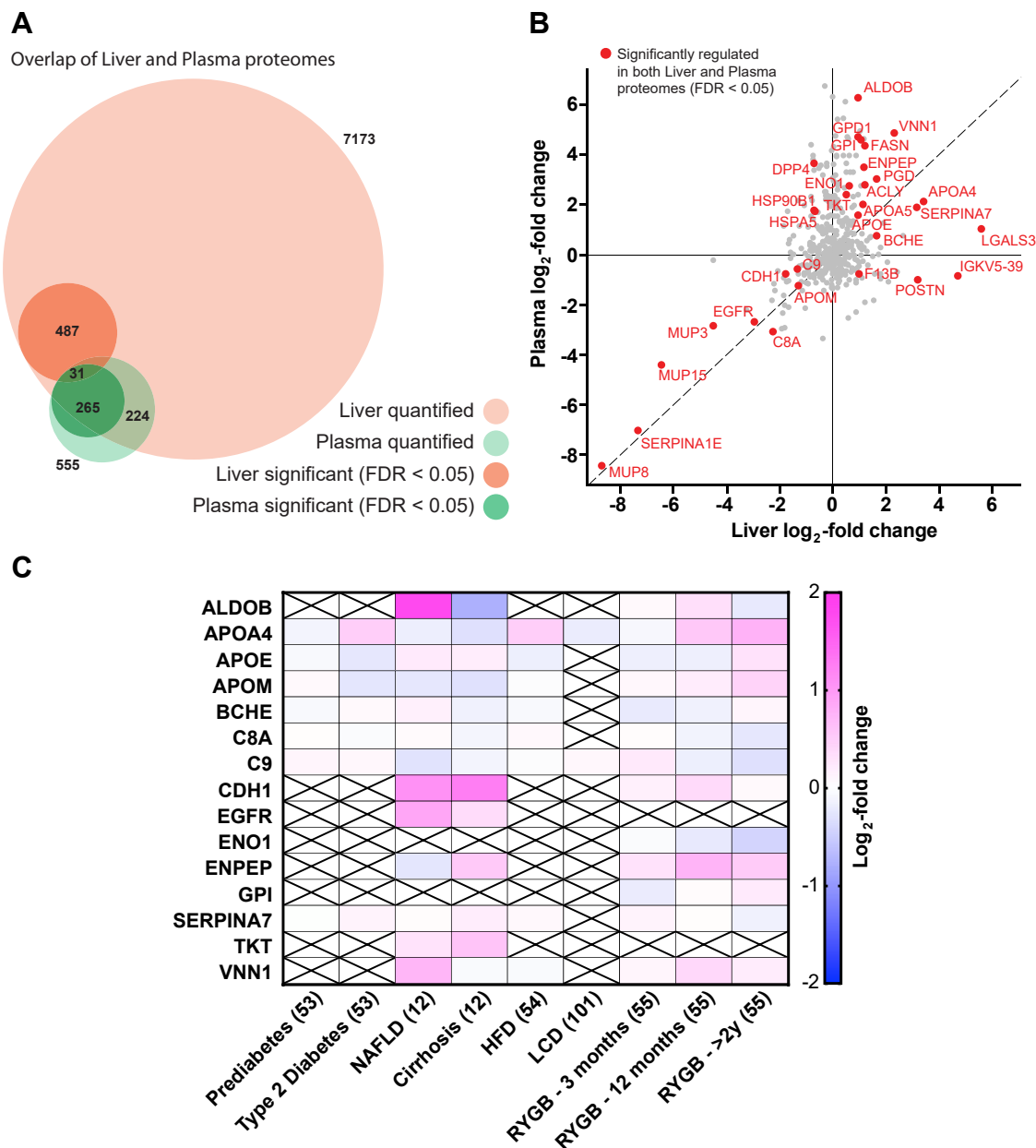

FIG. 7. **Integrated liver and plasma proteomics reveal concomitantly regulated proteins in the liver and plasma of *ob/ob* mice.** *A*, Venn diagram displaying the overlap of quantified and significantly regulated proteins in the liver and plasma proteomes. *B*, scatter plot of the log$_2$-fold-change in the liver and plasma of proteins quantified in both proteomes. Proteins significantly regulated in both proteomes are highlighted in *red*. *C*, heat map displaying the systemic (plasma or serum) regulation of proteins found to be concomitantly regulated in liver and plasma of *ob/ob* mice in human investigations of prediabetes and type diabetes (53), nonalcoholic fatty liver disease (NAFLD) and cirrhosis (12), high-fat diet (HFD) (54), low-calorie diet (LCD) (97), and Roux-en-Y gastric bypass (RYGB) (55).

in both datasets (Fig. 7B and supplemental Table S15). This allowed us to identify proteins whose abundance changed in the same direction in liver and plasma (Fig. 7B), suggesting a coordinated regulation during obesity. This analysis identified the concomitant downregulation of the liver-secreted membrane attack complex proteins C8A and C9 (Fig. 7B). Proteins involved in glucose (glucose-6-phosphate isomerase; GPI) and glycerol (GPD1) metabolism were upregulated in both datasets. Vanin 1 (VNN1), an enzyme involved in oxidative stress, coenzyme A metabolism, and lipid metabolism was also upregulated in both datasets. Proteins changing in the same direction in liver and plasma also included apolipoproteins (APOA4, APOE, and APOM), serpin proteins (SERPINA7 and SERPINA1E), and EGFR (Fig. 7B). To investigate whether these concomitantly regulated proteins are also regulated at the transcriptional level in the liver of ob/ob mice, we took advantage of the published transcriptomic dataset from ob/ob liver used in Figure 5 (41). The majority of the concomitantly regulated proteins displayed significant changes in transcription (supplemental Fig. S7) that mirrored changes in the liver and plasma proteomes (Fig. 7B). However, ALDOB and APOA5 did not change at the transcriptional level (supplemental Fig. S7), reflecting that the plasma concentration of ALDOB is indicative of hepatocyte damage, rather than a regulated process of transcription and secretion.

To identify whether these putatively liver-derived plasma proteins are relevant to human metabolic disease we investigated how these proteins were regulated in plasma and serum proteomes from human cohorts (Fig. 7C). Similarly to in the plasma of ob/ob mice, APOA4 increased in the serum of individuals with type 2 diabetes but not prediabetes (53); furthermore, APOA4 displayed a trend to increase after 6 weeks of HFD (54). ALDOB and VNN1 are increased in the plasma of individuals with NAFLD (12), whereas ALDOB is reduced after 2 years of Roux-en-Y gastric bypass-induced weight loss (55). These data indicate the clinical relevance of liver–plasma cross talk and our investigations in ob/ob mice.

DISCUSSION

Obesity is one of the world's largest healthcare challenges. Obesity leads to a dysregulated hepatic metabolism and to an excess deposition of lipids in the liver, known as steatosis (1). Here, we integrated liver and plasma proteomics in leptin-deficient obese (ob/ob) mice. Our analyses illuminated the complexity of hepatic peroxisomal proliferation and protein secretion during obesity. Furthermore, we identified substantial dysregulation of the plasma proteome in ob/ob mice, particularly of proteins involved in lipid and cholesterol metabolism, protein catabolism, and the immune system. Integration of the liver and plasma proteomes identified proteins whose differential plasma abundance is putatively regulated by altered liver expression and secretion, of which APOA4, ALDOB, and VNN1 are systemically regulated in the

development and/or treatment of human metabolic disease. Therefore, these integrated analyses provide biological insight into the alterations associated with obesity, as well as provide a comprehensive resource for obesity research in a prevailing model organism.

Obesity produced a predominant increase in proteins involved in hepatic lipid metabolism. Hyperphagia and excess energy intake lead to obesity and hepatic steatosis in ob/ob mice (24, 26). Our results suggest that this increase in lipid metabolism primarily results from peroxisomal proliferation with little effect on the mitochondrial proteome, which is in contrast to the skeletal muscle of these ob/ob mice in which increased mitochondrial protein content was apparent (27). We capitalized on the apparent peroxisomal proliferation and the deep coverage of the liver proteome to get an insight into peroxisomal biogenesis in the liver. Increased peroxisomal content occurs via de novo synthesis, and expansion and/or division of existing peroxisomes, which requires the import of peroxisomal membrane and matrix proteins. Import of newly synthesized peroxisomal membrane proteins occurs via two classes of mechanisms. In the class I mechanism, peroxisomal membrane proteins are targeted directly to the peroxisome from the cytosol in a PEX19-dependent manner, whereas the class II mechanism indirectly imports peroxisomal membrane proteins via a PEX16-mediated recruitment to the endoplasmic reticulum (45, 56). PEX19 increased in liver of ob/ob mice in the absence of changes to other proteins in the peroxisomal membrane import machinery (e.g., PEX3 or PEX16). Thus, the increase in PEX19, without an increase in PEX16, may indicate a predominance of class I peroxisomal membrane protein import in liver of obese mice. Initiation of peroxisomal matrix protein import occurs through recognition and binding of proteins containing peroxisomal targeting sequences (PTS) 1 and 2 by the cytosolic proteins PEX5 and PEX7, respectively (44). PEX5 and PEX7 then translocate PTS1- and PTS2-containing proteins to the PEX13-PEX14 docking complex, which transiently form an import pore (44). Here we report a significant increase in PEX14 in the liver of ob/ob mice, which raises the hypothesis that PEX14 is a rate-limiting protein in peroxisomal matrix protein import. Peroxisomal elongation and division is regulated by PEX11 proteins. Three PEX11 isoforms exist in mammalian cells, namely, the alpha (PEX11A), beta (PEX11B), and gamma (PEX11G) isoforms. Knockout of PEX11B is embryonically lethal, although it only moderately affects peroxisomal fatty acid oxidation (57). Conversely, Pex11a−/− mice are viable and they display impaired hepatic fatty acid oxidation and develop NAFLD (58). In the liver of ob/ob mice, PEX11A and PEX11G increased in the absence of changes to PEX11B. This corroborates previous evidence that PEX11A is an inducible gene, whereas PEX11B is constitutively expressed (59, 60). However, PEX11G, which is putatively constitutively expressed (61), is inducible during severe obesity. These data provide further evidence that PEX11 isoforms have distinct regulation and

function, implicating PEX11A and PEX11G in the metabolic adaptation to excess fatty acid availability.

Various components of secretory pathways were also dysregulated within *ob/ob* liver. In the classical secretion pathway, proteins with a signal peptide are targeted to the endoplasmic reticulum and transported *via* a multistep vesicular-mediated mechanism through the Golgi apparatus and released into the extracellular space through vesicular fusion with the plasma membrane (48). Greater than 10% of proteins containing a signal peptide were differentially regulated in liver of *ob/ob* mice. Furthermore, the summed protein abundance of the endoplasmic reticulum was decreased alongside the enrichment of the GOCC term *endoplasmic reticulum chaperone complex* among the downregulated proteins. The lumen of the endoplasmic reticulum, and particularly the chaperone proteins, provides a specialized environment for folding and maturation of secreted proteins (62). Endoplasmic reticulum stress is a common feature of obesity and NAFLD; however, this is typically characterized by an upregulation of chaperone genes (63). However, consistent with a reduction in protein content the mRNA expression of endoplasmic reticulum chaperon complex genes typically decreases in *ob/ob* mice (41), although the mRNA expression of BiP (HSPA5) has also been shown to increase (64, 65). It could be hypothesized that a reduction in protein abundance of endoplasmic reticulum chaperone proteins contributes to altered hepatic protein secretion, through increased misfolding of proteins that were destined for secretion. Proteins can also be secreted *via* endoplasmic reticulum–independent, nonclassical mechanisms, including *via* the release of exosomes (51). Proteins annotated to the extracellular exosome (GOCC) were enriched within the upregulated proteins. Nonetheless, several exosome-annotated proteins were downregulated, including proteins forming the membrane attack complex of the immune system. *Extracellular matrix* (GOCC) was also enriched within the upregulated proteins and transcripts of *ob/ob* mice, which contrasted with a down-regulation of extracellular matrix terms in the proteome of HFD-fed mice (42). However, extracellular matrix deposition has been described in the liver of HFD-fed mice elsewhere, whereby increased hepatic staining of alpha-smooth muscle actin is apparent, as well as increased gene expression of the type I and type II collagen molecules (66–68). Furthermore, both portal and perisinusoidal fibrosis are apparent in *ob/ob* mice fed a standard chow diet (26, 69). In addition to collagen deposition, we identified the upregulation of fibrillin 1, fibronectin, and laminin, as well as several secreted proteins that are annotated to the extracellular matrix (*e.g.*, APOE, LGALS1, LGALS3, and POSTN). Together, these data indicated a dysregulation of secreted proteins and the secretory machinery within the liver and led us to investigate whether these derangements altered the plasma proteome of *ob/ob* mice.

The plasma proteome of *ob/ob* mice displayed substantial regulation, whereby over half of the quantified proteins were differentially regulated. This is a somewhat larger proportion of the proteome than for HFD-fed mice, in which 30% of the plasma proteome is differentially regulated (70), consistent with a greater degree of obesity in *ob/ob* mice. Differentially regulated proteins included the potential NAFLD biomarkers ALDOB, APOE, DPP4, PIGR, and APOM identified in humans (12). Enriched within the upregulated proteins were GOBP terms relating to lipid and cholesterol homeostasis, which is in line with obesity-induced dyslipidemia (71). Furthermore, GOBP terms related to catabolism and the proteasome were also enriched among the upregulated proteins, whereas each protein of the 20S proteasome was increased in *ob/ob* plasma. The 26S proteasome, of which the 20S proteasome is a subunit, degrades the majority of cellular proteins. Although the role and source of the extracellular proteasome is less clear (72), the circulating proteasome is enzymatically functional (73) and has been identified in the human plasma proteome (55). Indeed, the extracellular proteasome may still be related to the degradation of short-lived and misfolded proteins, or alternatively it simply may represent a product of damaged cells. Nonetheless, the extracellular accumulation of damaged proteins has been associated with various disease states, including in a mouse model of type 2 diabetes (74). Furthermore, emerging evidence indicates circulating proteasome activity is negatively correlated with physical activity in individuals with chronic obstructive pulmonary disease (75) and positively correlated with squamous cell carcinoma (skin cancer) (76), indicating its clinical relevance. Future studies should investigate the relevance of elevated plasma proteasome abundance in the context of metabolic dysfunction and human obesity.

Enriched within the downregulated plasma proteins was the KEGG term *coagulation and complement cascade*, implicating hemostatic and immune system dysfunction in obesity. The reduction in plasma abundance of thrombotic proteins (*e.g.*, the fibrinogens FGA, FGB, and FGG and factor VII [F7]) is at odds with elevations in circulating prothrombotic factors and hypercoagulation in human obesity and type 2 diabetes (77–79). Nonetheless, this is in agreement with data identifying impaired platelet function and coagulation in leptin-deficient *ob/ob* mice (80). These data highlight the need to carefully choose a model organism dependent upon the specific aspect or stage of obesity that is to be studied. Nonetheless, we were interested by the observation that proteins from the membrane attack complex, the terminal complex of the complement cascade, were downregulated in both the liver and the plasma. Indeed, C8A and C9 were downregulated to a similar degree in both liver and plasma. Given the predominant expression of these proteins in the liver (81), plasma levels appear to be governed by altered secretion from the liver.

To identify additional proteins whose plasma regulation is likely influenced by altered abundance and secretion from the liver we integrated the liver and plasma proteomes. We identified 31 proteins that were significantly regulated in both liver

and plasma, of which 25 were regulated in the same direction, including proteins of the *complement and coagulation cascades*: C8A, C9, SERPINA1E, and SERPINA7. The NAFLD marker ALDOB was upregulated in both datasets, whereas DPP4 was upregulated in the plasma but downregulated in the liver. Furthermore, the apolipoproteins APOA4, APOA5, APOE, and APOM were also regulated in the same direction in liver and plasma. Interesting, the obesity-induced alteration in plasma abundance of a number of the proteins identified here as concomitantly regulated in the liver and plasma by obesity (*e.g.*, ALDOB, APOE, APOM, EGFR, SERPINA1E, and SER-PIN7) can be reversed by exercise training (70). Plasma ALDOB and VNN1 also increase in humans with NAFLD (12), whereas elevated plasma ALDOB can be reversed by sustained weight loss induced by Roux-en-Y gastric bypass (55). Furthermore, serum APOA4 is increased during type 2 diabetes and the consumption of a HFD in humans (53, 54), suggesting it is a sensitive systemic marker of altered liver metabolism. LGALS3, which lacks a signal peptide (82), was also identified as one of the most upregulated exosome-annotated proteins in the liver and was also upregulated in the plasma. In humans, plasma LGALS3 correlates with disease states such as type 2 diabetes and cardiovascular disease (83–85) and is an emerging therapeutic target for treating NAFLD (86). LGALS3 is profibrotic (87, 88) and immune modulatory (89), regulating the extracellular matrix of numerous tissues, including the cardiac tissue of patients with heart failure (90). Although increased LGALS3 expression is not exclusive to the liver during obesity (91), our data does indicate that the liver is a source, or potentially a target (87), of altered systemic LGALS3 abundance in obesity. Together, these data identify clinically relevant liver-derived plasma proteins in obesity and indicate that the *ob/ob* mouse is a useful model of liver–plasma cross talk in hepatic dysfunction.

One limitation of this investigation is that *ob/ob* mice are a monogenic model of obesity, harboring a mutation in the leptin gene resulting in a truncated nonfunctional protein (21), which is in contrast to the vast majority of cases of human obesity, in which circulating levels of leptin increase (92). Some phenotypic and proteomic aspects of obesity in *ob/ob* mice will be directly due to the loss of functional leptin, rather than an outcome of obesity. For example, leptin reduces the expression of SCD1, the rate-limiting enzyme in the biosynthesis of monounsaturated fatty acids (93), whereas leptin *per se* is immunoregulatory (94). Indeed, the poor correlation between the liver proteomes of *ob/ob* and HFD-fed mice further highlights the issue of translating findings from a single model of obesity, albeit many processes were commonly regulated between *ob/ob* and HFD-fed mice when viewed at a systems level (*e.g.*, fatty acid metabolism, glycolysis and gluconeogenesis, and peroxisomal biogenesis). Nonetheless, the *ob/ob* mouse remains a useful model for obesity research (20). Furthermore, individuals with mutations in the human leptin gene have

been identified, which is also associated with severe early onset of obesity (95). Thus, our proteomic investigation of the *ob/ob* mouse may also have relevance to a rare congenital form of leptin-deficient obesity.

By quantifying the abundance of 7173 and 555 proteins within the liver and plasma of obese leptin-deficient *ob/ob* mice, respectively, we illuminated the complexity of adaptations during severe obesity. Within the liver, fatty acid metabolism, peroxisomal biogenesis, and the secretory pathways were dysregulated. Furthermore, we identified the substantial dysregulation of the plasma proteome in *ob/ob* mice, whereby more than 50% of the quantified plasma proteins were differentially regulated, identifying metabolic, proteasomal, and immune system dysregulation. Furthermore, by integrating the liver and plasma proteomes, we identified concomitantly regulated proteins with clinical relevance to human metabolic diseases. In addition to these biological insights, these analyses provide a comprehensive resource in the study of obesity.

DATA AVAILABILITY

The mass spectrometry proteomics data produced in this investigation, including peptide and protein level identifications, have been deposited to the ProteomeXchange Consortium *via* the PRIDE partner repository (96) (http://www.proteomexchange.org/) with the accession number PXD026821. The in-house library used for the quantification of the plasma proteome has previously been deposited to PRIDE with the identifier PXD017170 (33). Annotated spectra of data-dependent acquisition data can be visualized using the MS-Viewer in ProteinProspector with the search key t2hr4mzs7d: http://msviewer.ucsf.edu:443/prospector/cgi-bin/mssearch.cgi?report_title=MS-Viewer&search_key=t2hr4mzs7d&search_name=msviewer.

Abbreviations—The abbreviations used are: DIA, data-independent acquisition; FDR, false discovery rate; GO, gene ontology; GOBP, gene ontology biological processes; GOCC, gene ontology cellular compartment; HFD, high-fat diet; KEGG, Kyoto encyclopedia of genes and genomes; LC-MS/MS, liquid chromatography–tandem mass spectrometry; MED-FASP, multienzyme digestion with filter-aided sample preparation; NAFLD, nonalcoholic fatty liver disease; PTS, peroxisomal targeting sequences; TPA, total protein abundance.

REFERENCES

1. Kawano, Y., and Cohen, D. E. (2013) Mechanisms of hepatic triglyceride accumulation in non-alcoholic fatty liver disease. *J. Gastroenterol.* **48**, 434–441
2. Cohen, J. C., Horton, J. D., and Hobbs, H. H. (2011) Human fatty liver disease: Old questions and new insights. *Science* **332**, 1519–1523
3. Gruben, N., Shiri-Sverdlov, R., Koonen, D. P. Y., and Hofker, M. H. (2014) Nonalcoholic fatty liver disease: A main driver of insulin resistance or a dangerous liaison? *Biochim. Biophys. Acta* **1842**, 2329–2343
4. Knobler, H., Schattner, A., Zhornicki, T., Malnick, S. D., Keter, D., Sokolovskaya, N., Lurie, Y., and Bass, D. D. (1999) Fatty liver–an additional and treatable feature of the insulin resistance syndrome. *QJM* **92**, 73–79
5. Utzschneider, K. M., and Kahn, S. E. (2006) The role of insulin resistance in nonalcoholic fatty liver disease. *J. Clin. Endocrinol. Metab.* **91**, 4753–4761
6. Organization, W. H. (2014) *Global Status Report on Noncommunicable Diseases 2014*. World Health Organization, Geneva
7. Bellentani, S., Scaglioni, F., Marino, M., and Bedogni, G. (2010) Epidemiology of non-alcoholic fatty liver disease. *Dig. Dis.* **28**, 155–161
8. Fan, J. G., Kim, S. U., and Wong, V. W. (2017) New trends on obesity and NAFLD in Asia. *J. Hepatol.* **67**, 862–873
9. Hotamisligil, G. S. (2006) Inflammation and metabolic disorders. *Nature* **444**, 860–867
10. Shoelson, S. E., Lee, J., and Goldfine, A. B. (2006) Inflammation and insulin resistance. *J. Clin. Invest.* **116**, 1793–1801
11. Hotamisligil, G. S., Shargill, N. S., and Spiegelman, B. M. (1993) Adipose expression of tumor necrosis factor-alpha: Direct role in obesity-linked insulin resistance. *Science* **259**, 87
12. Niu, L., Geyer, P. E., Wewer Albrechtsen, N. J., Gluud, L. L., Santos, A., Doll, S., Treit, P. V., Holst, J. J., Knop, F. K., Vilsboll, T., Junker, A., Sachs, S., Stemmer, K., Muller, T. D., Tschop, M. H., *et al.* (2019) Plasma proteome profiling discovers novel proteins associated with nonalcoholic fatty liver disease. *Mol. Syst. Biol.* **15**, e8793
13. Anstey, K. J., Cherbuin, N., Budge, M., and Young, J. (2011) Body mass index in midlife and late-life as a risk factor for dementia: A meta-analysis of prospective studies. *Obes. Rev.* **12**, e426–e437
14. Calle, E. E., Thun, M. J., Petrelli, J. M., Rodriguez, C., and Heath, C. W. (1999) Body-mass index and mortality in a prospective cohort of U.S. adults. *N. Engl. J. Med.* **341**, 1097–1105
15. Calle, E. E., Rodriguez, C., Walker-Thurmond, K., and Thun, M. J. (2003) Overweight, obesity, and mortality from cancer in a prospectively studied cohort of U.S. adults. *N. Engl. J. Med.* **348**, 1625–1638
16. Nho, K., Kueider-Paisley, A., Ahmad, S., MahmoudianDehkordi, S., Arnold, M., Risacher, S. L., Louie, G., Blach, C., Baillie, R., Han, X., Kastenmüller, G., Trojanowski, J. Q., Shaw, L. M., Weiner, M. W., Doraiswamy, P. M., *et al.* (2019) Association of altered liver enzymes with Alzheimer disease diagnosis, cognition, neuroimaging measures, and cerebrospinal fluid biomarkers. *JAMA Netw. Open* **2**, e197978
17. Bassendine, M. F., Taylor-Robinson, S. D., Fertleman, M., Khan, M., and Neely, D. (2020) Is Alzheimer's disease a liver disease of the brain? *J. Alzheimers Dis.* **75**, 1–14
18. Sorensen, H. T., Friis, S., Olsen, J. H., Thulstrup, A. M., Mellemkjaer, L., Linet, M., Trichopoulos, D., Vilstrup, H., and Olsen, J. (1998) Risk of liver and other types of cancer in patients with cirrhosis: A nationwide cohort study in Denmark. *Hepatology* **28**, 921–925
19. Targher, G., Bertolini, L., Rodella, S., Tessari, R., Zenari, L., Lippi, G., and Arcaro, G. (2007) Nonalcoholic fatty liver disease is independently associated with an increased incidence of cardiovascular events in type 2 diabetic patients. *Diabetes Care* **30**, 2119
20. Barrett, P., Mercer, J. G., and Morgan, P. J. (2016) Preclinical models for obesity research. *Dis. Model. Mech.* **9**, 1245
21. Zhang, Y., Proenca, R., Maffei, M., Barone, M., Leopold, L., and Friedman, J. M. (1994) Positional cloning of the mouse obese gene and its human homologue. *Nature* **372**, 425–432
22. Mayer, J., Bates, M. W., and Dickie, M. M. (1951) Hereditary diabetes in genetically obese mice. *Science* **113**, 746–747
23. Mayer, J., Dickie, M. M., Bates, M. W., and Vitale, J. J. (1951) Free selection of nutrients by hereditarily obese mice. *Science* **113**, 745–746
24. Jéquier, E. (2002) Leptin signaling, adiposity, and energy balance. *Ann. N. Y. Acad. Sci.* **967**, 379–388
25. Dubuc, P. U. (1976) The development of obesity, hyperinsulinemia, and hyperglycemia in ob/ob mice. *Metabolism* **25**, 1567–1574
26. Trak-Smayra, V., Paradis, V., Massart, J., Nasser, S., Jebara, V., and Fromenty, B. (2011) Pathology of the liver in obese and diabetic ob/ob and db/db mice fed a standard or high-calorie diet. *Int. J. Exp. Pathol.* **92**, 413–421
27. Schonke, M., Bjornholm, M., Chibalin, A. V., Zierath, J. R., and Deshmukh, A. S. (2018) Proteomics analysis of skeletal muscle from leptin-deficient ob/ob mice reveals adaptive remodeling of metabolic characteristics and fiber type composition. *Proteomics* **18**, e1700375
28. Wisniewski, J. R., and Mann, M. (2012) Consecutive proteolytic digestion in an enzyme reactor increases depth of proteomic and phosphoproteomic analysis. *Anal. Chem.* **84**, 2631–2637
29. Rappsilber, J., Ishihama, Y., and Mann, M. (2003) Stop and go extraction tips for matrix-assisted laser desorption/ionization, nanoelectrospray, and LC/MS sample pretreatment in proteomics. *Anal. Chem.* **75**, 663–670
30. Geyer, P. E., Kulak, N. A., Pichler, G., Holdt, L. M., Teupser, D., and Mann, M. (2016) Plasma proteome profiling to assess human health and disease. *Cell Syst.* **2**, 185–195
31. Tyanova, S., Temu, T., and Cox, J. (2016) The MaxQuant computational platform for mass spectrometry-based shotgun proteomics. *Nat. Protoc.* **11**, 2301–2319
32. Bruderer, R., Bernhardt, O. M., Gandhi, T., Miladinović, S. M., Cheng, L. Y., Messner, S., Ehrenberger, T., Zanotelli, V., Butscheid, Y., Escher, C., Vitek, O., Rinner, O., and Reiter, L. (2015) Extending the limits of quantitative proteome profiling with data-independent acquisition and application to acetaminophen-treated three-dimensional liver microtissues. *Mol. Cell. Proteomics* **14**, 1400–1410
33. Dall, M., Hassing, A. S., Niu, L., Nielsen, T. S., Ingerslev, L. R., Sulek, K., Trammell, S. A. J., Gillum, M. P., Barrès, R., Larsen, S., Poulsen, S. S., Mann, M., Ørskov, C., and Treebak, J. T. (2021) Hepatocyte-specific perturbation of NAD+ biosynthetic pathways in mice induces reversible nonalcoholic steatohepatitis–like phenotypes. *J. Biol. Chem.* **297**, 101388
34. Storey, J. D., and Tibshirani, R. (2003) Statistical significance for genome-wide studies. *Proc. Natl. Acad. Sci. U. S. A.* **100**, 9440

35. Tyanova, S., Temu, T., Sinitcyn, P., Carlson, A., Hein, M. Y., Geiger, T., Mann, M., and Cox, J. (2016) The Perseus computational platform for comprehensive analysis of (prote)omics data. *Nat. Methods* **13**, 731

36. Wisniewski, J. R. (2017) Label-free and standard-free absolute quantitative proteomics using the "total protein" and "proteomic ruler" approaches. *Methods Enzymol.* **585**, 49–60

37. Wiśniewski, J. R., Hein, M. Y., Cox, J., and Mann, M. (2014) A "proteomic ruler" for protein copy number and concentration estimation without spike-in standards. *Mol. Cell. Proteomics* **13**, 3497–3506

38. Tusher, V. G., Tibshirani, R., and Chu, G. (2001) Significance analysis of microarrays applied to the ionizing radiation response. *Proc. Natl. Acad. Sci. U. S. A.* **98**, 5116–5121

39. Bindea, G., Mlecnik, B., Hackl, H., Charoentong, P., Tosolini, M., Kirilovsky, A., Fridman, W.-H., Pagès, F., Trajanoski, Z., and Galon, J. (2009) ClueGO: A cytoscape plug-in to decipher functionally grouped gene ontology and pathway annotation networks. *Bioinformatics* **25**, 1091–1093

40. Cox, J., and Mann, M. (2012) 1D and 2D annotation enrichment: A statistical method integrating quantitative proteomics with complementary high-throughput data. *BMC Bioinformatics* **13**, S12

41. Egami, R., Kokaji, T., Hatano, A., Yugi, K., Eto, M., Morita, K., Ohno, S., Fujii, M., Hironaka, K. I., Uematsu, S., Terakawa, A., Bai, Y., Pan, Y., Tsuchiya, T., Ozaki, H., *et al.* (2021) Trans-omic analysis reveals obesity-associated dysregulation of inter-organ metabolic cycles between the liver and skeletal muscle. *iScience* **24**, 102217

42. Krahmer, N., Najafi, B., Schueder, F., Quagliarini, F., Steger, M., Seitz, S., Kasper, R., Salinas, F., Cox, J., Uhlenhaut, N. H., Walther, T. C., Jungmann, R., Zeigerer, A., Borner, G. H. H., and Mann, M. (2018) Organellar proteomics and phospho-proteomics reveal subcellular reorganization in diet-induced hepatic steatosis. *Dev. Cell* **47**, 205–221.e7

43. Gonzalez-Franquesa, A., Stocks, B., Borg, M. L., Kuefner, M., Dalbram, E., Nielsen, T. S., Agrawal, A., Pankratova, S., Chibalin, A. V., Karlsson, H. K. R., Gheibi, S., Björnholm, M., Jørgensen, N. R., Clemmensen, C., Hostrup, M., *et al.* (2021) Discovery of thymosin β4 as a human exerkine and growth factor. *Am. J. Physiol. Cell Physiol.* **321**, C770–C778

44. Fujiki, Y., Okumoto, K., Mukai, S., Honsho, M., and Tamura, S. (2014) Peroxisome biogenesis in mammalian cells. *Front. Physiol.* **5**, 307

45. Jones, J. M., Morrell, J. C., and Gould, S. J. (2004) PEX19 is a predominantly cytosolic chaperone and import receptor for class 1 peroxisomal membrane proteins. *J. Cell Biol.* **164**, 57–67

46. Koch, J., and Brocard, C. (2012) PEX11 proteins attract Mff and human Fis1 to coordinate peroxisomal fission. *J. Cell Sci.* **125**, 3813–3826

47. Walter, P., Gilmore, R., and Blobel, G. (1984) Protein translocation across the endoplasmic reticulum. *Cell* **38**, 5–8

48. Palade, G. (1975) Intracellular aspects of the process of protein synthesis. *Science* **189**, 347

49. Horras, C. J., Lamb, C. L., and Mitchell, K. A. (2011) Regulation of hepatocyte fate by interferon-γ. *Cytokine Growth Factor Rev.* **22**, 35–43

50. Volpes, R., van den Oord, J. J., De Vos, R., Depla, E., De Ley, M., and Desmet, V. J. (1991) Expression of interferon-γ receptor in normal and pathological human liver tissue. *J. Hepatol.* **12**, 195–202

51. Hessvik, N. P., and Llorente, A. (2018) Current knowledge on exosome biogenesis and release. *Cell. Mol. Life Sci.* **75**, 193–208

52. Henderson, N. C., Mackinnon, A. C., Farnworth, S. L., Poirier, F., Russo, F. P., Iredale, J. P., Haslett, C., Simpson, K. J., and Sethi, T. (2006) Galectin-3 regulates myofibroblast activation and hepatic fibrosis. *Proc. Natl. Acad. Sci. U. S. A.* **103**, 5060

53. [preprint] Diamanti, K., Cavalli, M., Pereira, M. J., Pan, G., Castillejo-Lopez, C., Kumar, C., Mundt, F., Komorowski, J., Deshmukh, A. S., Mann, M., Korsgren, O., Eriksson, J. W., and Wadelius, C. (2021) Organ-specific metabolic pathways distinguish prediabetes, type 2 diabetes and normal tissues. *bioRxiv*. https://doi.org/10.1101/2021.05.09.443296

54. Lundsgaard, A.-M., Holm, J. B., Sjøberg, K. A., Bojsen-Møller, K. N., Myrmel, L. S., Fjære, E., Jensen, B. A. H., Nicolaisen, T. S., Hingst, J. R., Hansen, S. L., Doll, S., Geyer, P. E., Deshmukh, A. S., Holst, J. J., Madsen, L., *et al.* (2019) Mechanisms preserving insulin action during high dietary fat intake. *Cell Metab.* **29**, 50–63.e54

55. Wewer Albrechtsen, N. J., Geyer, P. E., Doll, S., Treit, P. V., Bojsen-Møller, K. N., Martinussen, C., Jørgensen, N. B., Torekov, S. S., Meier, F., Niu, L., Santos, A., Keilhauer, E. C., Holst, J. J., Madsbad, S., and Mann, M.

(2018) Plasma proteome profiling reveals dynamics of inflammatory and lipid homeostasis markers after roux-en-Y gastric bypass surgery. *Cell Syst.* **7**, 601–612.e3

56. Aranovich, A., Hua, R., Rutenberg, A. D., and Kim, P. K. (2014) PEX16 contributes to peroxisome maintenance by constantly trafficking PEX3 *via* the ER. *J. Cell Sci.* **127**, 3675–3686

57. Li, X., Baumgart, E., Morrell, J. C., Jimenez-Sanchez, G., Valle, D., and Gould, S. J. (2002) PEX11 beta deficiency is lethal and impairs neuronal migration but does not abrogate peroxisome function. *Mol. Cell. Biol.* **22**, 4358–4365

58. Weng, H., Ji, X., Naito, Y., Endo, K., Ma, X., Takahashi, R., Shen, C., Hirokawa, Y., Fukushima, Y., and Iwai, N. (2012) Pex11α deficiency impairs peroxisome elongation and division and contributes to nonalcoholic fatty liver in mice. *Am. J. Physiol. Endocrinol. Metab.* **304**, E187–E196

59. Abe, I., and Fujiki, Y. (1998) cDNA cloning and characterization of a constitutively expressed isoform of the human peroxin Pex11p. *Biochem. Biophys. Res. Commun.* **252**, 529–533

60. Abe, I., Okumoto, K., Tamura, S., and Fujiki, Y. (1998) Clofibrate-inducible, 28-kDa peroxisomal integral membrane protein is encoded by PEX11. *FEBS Lett.* **431**, 468–472

61. Tanaka, A., Okumoto, K., and Fujiki, Y. (2003) cDNA cloning and characterization of the third isoform of human peroxin Pex11p. *Biochem. Biophys. Res. Commun.* **300**, 819–823

62. Braakman, I., and Hebert, D. N. (2013) Protein folding in the endoplasmic reticulum. *Cold Spring Harb. Perspect. Biol.* **5**, a013201

63. Pagliassotti, M. J., Kim, P. Y., Estrada, A. L., Stewart, C. M., and Gentile, C. L. (2016) Endoplasmic reticulum stress in obesity and obesity-related disorders: An expanded view. *Metabolism* **65**, 1238–1246

64. Kammoun, H. L., Chabanon, H., Hainault, I., Luquet, S., Magnan, C., Koike, T., Ferré, P., and Foufelle, F. (2009) GRP78 expression inhibits insulin and ER stress-induced SREBP-1c activation and reduces hepatic steatosis in mice. *J. Clin. Invest.* **119**, 1201–1215

65. Özcan, U., Cao, Q., Yilmaz, E., Lee, A.-H., Iwakoshi, N. N., Özdelen, E., Tuncman, G., Görgün, C., Glimcher, L. H., and Hotamisligil, G. S. (2004) Endoplasmic reticulum stress links obesity, insulin action, and type 2 diabetes. *Science* **306**, 457

66. Wada, T., Miyashita, Y., Sasaki, M., Aruga, Y., Nakamura, Y., Ishii, Y., Sasahara, M., Kanasaki, K., Kitada, M., Koya, D., Shimano, H., Tsuneki, H., and Sasaoka, T. (2013) Eplerenone ameliorates the phenotypes of metabolic syndrome with NASH in liver-specific SREBP-1c Tg mice fed high-fat and high-fructose diet. *Am. J. Physiol. Endocrinol. Metab.* **305**, E1415–E1425

67. Dixon, L. J., Flask, C. A., Papouchado, B. G., Feldstein, A. E., and Nagy, L. E. (2013) Caspase-1 as a central regulator of high fat diet-induced nonalcoholic steatohepatitis. *PLoS One* **8**, e56100

68. Williams, A. S., Kang, L., Zheng, J., Grueter, C., Bracy, D. P., James, F. D., Pozzi, A., and Wasserman, D. H. (2015) Integrin α1-null mice exhibit improved fatty liver when fed a high fat diet despite severe hepatic insulin resistance. *J. Biol. Chem.* **290**, 6546–6557

69. Sutter, A. G., Palanisamy, A. P., Lench, J. H., Jessmore, A. P., and Chavin, K. D. (2015) Development of steatohepatitis in ob/ob mice is dependent on Toll-like receptor 4. *Ann. Hepatol.* **14**, 735–743

70. Martinez-Huenchullan, S. F., Shipsey, I., Hatchwell, L., Min, D., Twigg, S. M., and Larance, M. (2021) Blockade of high-fat diet proteomic phenotypes using exercise as prevention or treatment. *Mol. Cell. Proteomics* **20**, 100027

71. Klop, B., Elte, J. W. F., and Cabezas, M. C. (2013) Dyslipidemia in obesity: Mechanisms and potential targets. *Nutrients* **5**, 1218–1240

72. Dwivedi, V., Yaniv, K., and Sharon, M. (2021) Beyond cells: The extracellular circulating 20S proteasomes. *Biochim. Biophys. Acta Mol. Basis Dis.* **1867**, 166041

73. Zoeger, A., Blau, M., Egerer, K., Feist, E., and Dahlmann, B. (2006) Circulating proteasomes are functional and have a subtype pattern distinct from 20S proteasomes in major blood cells. *Clin. Chem.* **52**, 2079–2086

74. Wyatt, A. R., Yerbury, J. J., Poon, S., and Wilson, M. R. (2009) Therapeutic targets in extracellular protein deposition diseases. *Curr. Med. Chem.* **16**, 2855–2866

75. Lee, K. Y., Chen, T. T., Chiang, L. L., Chuang, H. C., Feng, P. H., Liu, W. T., Chen, K. Y., and Ho, S. C. (2017) Proteasome activity related with the daily physical activity of COPD patients. *Int. J. Chron. Obstruct. Pulmon. Dis.* **12**, 1519–1525

76. Kakurina, G. V., Cheremisina, O. V., Choinzonov, E. L., and Kondakova, I. V. (2017) Circulating proteasomes in the pathogenesis of head and neck squamous cell carcinoma. *Bull. Exp. Biol. Med.* **163**, 92–94

77. Carr, M. E. (2001) Diabetes mellitus: A hypercoagulable state. *J. Diabetes Complications* **15**, 44–54

78. Kaye, S. M., Pietiläinen, K. H., Kotronen, A., Joutsi-Korhonen, L., Kaprio, J., Yki-Järvinen, H., Silveira, A., Hamsten, A., Lassila, R., and Rissanen, A. (2012) Obesity-related derangements of coagulation and fibrinolysis: A study of obesity-discordant monozygotic twin pairs. *Obesity* **20**, 88–94

79. De Pergola, G., De Mitrio, V., Giorgino, F., Sciaraffia, M., Minenna, A., Di Bari, L., Pannacciulli, N., and Giorgino, R. (1997) Increase in both prothrombotic and anti-thrombotic factors in obese premenopausal women: Relationship with body fat distribution. *Int. J. Obes. Relat. Metab. Disord.* **21**, 527–535

80. Henry, M. L., Davidson, L. B., Wilson, J. E., McKenna, B. K., Scott, S. A., McDonagh, P. F., and Ritter, L. S. (2008) Whole blood aggregation and coagulation in db/db and ob/ob mouse models of type 2 diabetes. *Blood Coagul. Fibrinolysis* **19**, 124–134

81. Uhlén, M., Fagerberg, L., Hallström, B. M., Lindskog, C., Oksvold, P., Mardinoglu, A., Sivertsson, Å., Kampf, C., Sjöstedt, E., Asplund, A., Olsson, I., Edlund, K., Lundberg, E., Navani, S., Szigyarto, C. A., *et al*. (2015) Proteomics. Tissue-based map of the human proteome. *Science* **347**, 1260419

82. Menon, R. P., and Hughes, R. C. (1999) Determinants in the N-terminal domains of galectin-3 for secretion by a novel pathway circumventing the endoplasmic reticulum-Golgi complex. *Eur. J. Biochem.* **264**, 569–576

83. van Kimmenade, R. R., Januzzi, J. L., Jr., Ellinor, P. T., Sharma, U. C., Bakker, J. A., Low, A. F., Martinez, A., Crijns, H. J., MacRae, C. A., Menheere, P. P., and Pinto, Y. M. (2006) Utility of amino-terminal pro-brain natriuretic peptide, galectin-3, and apelin for the evaluation of patients with acute heart failure. *J. Am. Coll. Cardiol.* **48**, 1217–1224

84. van der Velde, A. R., Gullestad, L., Ueland, T., Aukrust, P., Guo, Y., Adourian, A., Muntendam, P., van Veldhuisen, D. J., and de Boer, R. A. (2013) Prognostic value of changes in galectin-3 levels over time in patients with heart failure: Data from CORONA and COACH. *Circ. Heart Fail.* **6**, 219–226

85. Weigert, J., Neumeier, M., Wanninger, J., Bauer, S., Farkas, S., Scherer, M. N., Schnitzbauer, A., Schäffler, A., Aslanidis, C., Schölmerich, J., and Buechler, C. (2010) Serum galectin-3 is elevated in obesity and negatively correlates with glycosylated hemoglobin in type 2 diabetes. *J. Clin. Endocrinol. Metab.* **95**, 1404–1411

86. Al Attar, A., Antaramian, A., and Noureddin, M. (2021) Review of galectin-3 inhibitors in the treatment of nonalcoholic steatohepatitis. *Expert Rev. Clin. Pharmacol.* **14**, 457–464

87. Jeftic, I., Jovicic, N., Pantic, J., Arsenijevic, N., Lukic, M. L., and Pejnovic, N. (2015) Galectin-3 ablation enhances liver steatosis, but attenuates inflammation and IL-33-dependent fibrosis in obesogenic mouse model of nonalcoholic steatohepatitis. *Mol. Med.* **21**, 453–465

88. Yu, L., Ruifrok Willem, P. T., Meissner, M., Bos Eelke, M., van Goor, H., Sanjabi, B., van der Harst, P., Pitt, B., Goldstein Irwin, J., Koerts Jasper, A., van Veldhuisen Dirk, J., Bank Ruud, A., van Gilst Wiek, H., Silljé Herman, H. W., and de Boer Rudolf, A. (2013) Genetic and pharmacological inhibition of galectin-3 prevents cardiac remodeling by interfering with myocardial fibrogenesis. *Circ. Heart Fail.* **6**, 107–117

89. Dumic, J., Dabelic, S., and Flögel, M. (2006) Galectin-3: An open-ended story. *Biochim. Biophys. Acta* **1760**, 616–635

90. Lin, Y. H., Lin, L. Y., Wu, Y. W., Chien, K. L., Lee, C. M., Hsu, R. B., Chao, C. L., Wang, S. S., Hsein, Y. C., Liao, L. C., Ho, Y. L., and Chen, M. F. (2009) The relationship between serum galectin-3 and serum markers of cardiac extracellular matrix turnover in heart failure patients. *Clin. Chim. Acta* **409**, 96–99

91. Papaspyridonos, M., McNeill, E., de Bono Joe, P., Smith, A., Burnand Kevin, G., Channon Keith, M., and Greaves David, R. (2008) Galectin-3 is an amplifier of inflammation in atherosclerotic plaque progression through macrophage activation and monocyte chemoattraction. *Arterioscler. Thromb. Vasc. Biol.* **28**, 433–440

92. Considine, R. V., Sinha, M. K., Heiman, M. L., Kriauciunas, A., Stephens, T. W., Nyce, M. R., Ohannesian, J. P., Marco, C. C., McKee, L. J., Bauer, T. L., and Caro, J. F. (1996) Serum immunoreactive-leptin concentrations in normal-weight and obese humans. *N. Engl. J. Med.* **334**, 292–295

93. Biddinger, S. B., Miyazaki, M., Boucher, J., Ntambi, J. M., and Kahn, C. R. (2006) Leptin suppresses stearoyl-CoA desaturase 1 by mechanisms independent of insulin and sterol regulatory element-binding protein-1c. *Diabetes* **55**, 2032–2041

94. Naylor, C., and Petri, W. A., Jr. (2016) Leptin regulation of immune responses. *Trends Mol. Med.* **22**, 88–98

95. Montague, C. T., Farooqi, I. S., Whitehead, J. P., Soos, M. A., Rau, H., Wareham, N. J., Sewter, C. P., Digby, J. E., Mohammed, S. N., Hurst, J. A., Cheetham, C. H., Earley, A. R., Barnett, A. H., Prins, J. B., and O'Rahilly, S. (1997) Congenital leptin deficiency is associated with severe early-onset obesity in humans. *Nature* **387**, 903–908

96. Perez-Riverol, Y., Csordas, A., Bai, J., Bernal-Llinares, M., Hewapathirana, S., Kundu, D. J., Inuganti, A., Griss, J., Mayer, G., Eisenacher, M., Perez, E., Uszkoreit, J., Pfeuffer, J., Sachsenberg, T., Yilmaz, S., *et al* (2019) The PRIDE database and related tools and resources in 2019: Improving support for quantification data. *Nucleic Acids Res.* **47**, D442–D450

97. Geyer, P. E., Wewer Albrechtsen, N. J., Tyanova, S., Grassl, N., Iepsen, E. W., Lundgren, J., Madsbad, S., Holst, J. J., Torekov, S. S., and Mann, M. (2016) Proteomics reveals the effects of sustained weight loss on the human plasma proteome. *Mol. Syst. Biol.* **12**, 901